A Search for Anomalous Top Production at H1

Ronald Weber

Diploma thesis

supervised by
Prof. Dr. R. A. Eichler

Tutor: Dr. C. Grab

Institute for Particle Physics
ETH - Zürich

Switzerland

September 13th 2001

Diese Arbeit ist
meiner Grossmutter gewidmet

Contents

1 Introduction **3**

2 An Introduction to the Theory **5**
2.1 General Kinematics of ep Reactions 5
2.2 Deep Inelastic ep-scattering in the Parton Model 7
2.3 Photoproduction 8
2.4 Anomalous Top Production and its decay modes 9
2.5 ep collisions at HERA 11

3 Experimental Setup **13**
3.1 The HERA Collider 13
3.2 H1 Detector 14
3.2.1 Tracking Chamber 16
3.2.2 Liquid Argon Calorimeter (LAr) 18
3.2.3 Superconducting Coil and Iron Yoke 20
3.2.4 Trigger System and Reconstruction 20
3.3 Luminosity System 22

4 Monte Carlo and Background **23**
4.1 Anomalous Top Production Monte Carlo 23
4.2 Background 25
4.2.1 Non ep Background 25
4.2.2 SM W Production (γp) 25
4.2.3 Lepton Pair Production ($\gamma\gamma$) 26
4.2.4 Standard Model Jets (γp) and Single π-Jets 27
4.2.5 Anomolous top decay in muons 27

5 Event Selection **29**
5.1 Principle of the analysis 29
5.2 Reconstruction of the Event 30
5.3 The Jet Algorithm *QJCONE* 31
5.3.1 Definition of the Jet 31
5.3.2 Reconstruction of the τ Jet 33
5.4 Sensitive kinematical variables for Anomalous Top Production 33

5.5 The Preselection 36
5.6 Final Analysis 37
5.7 Calculating the Efficiency 45
5.8 Result 46

6 The Cross Section for Anomalous Top Production 47
6.1 Production Cross Section 47
6.2 Upper Limit 48
6.2.1 Background Estimation 49

7 Conclusion and Outlook 51

8 Acknowledgments 53

A Event Display 55

Abstract

A search for Anomalous Top Production mediated by a flavour changing neutral current was performed in ep collisions at HERA. The search examined data collected with the H1 detector from 1999 and 2000 with an integrated luminosity of 62.76 pb^{-1}. The analysis was motivated by the previous observation of outstanding events with isolated leptons, missing transverse momentum and a jet with large transverse momentum. The top decay is considered for the first time in the decay chain $t \to Wb$, $W \to \tau\nu_\tau$ and a hadronic final state. Within this decay channel no events were found to be compatible with the hypothesis of Anomalous Top Production. The resulting upper limit for the production cross section of Anomalous Top Production was calculated to be

$$\sigma(ep \to e'tX, \sqrt{s} = 320 \text{ GeV}) \leq 6.8 \ pb \qquad \text{at } 95 \ \% \text{ CL}$$

and supports the upper limit derived from the previous Anomalous Top Production searches at HERA in the electron and muon channel.

Chapter 1

Introduction

In todays High Energy Physics, the *Standard Model* (SM) is well accepted and has shown its validity up to ∼1000 GeV. But what happens beyond this energy, is subject to many new experiments and collaborations, such as LHC[1] at CERN[2] or TESLA[3] at DESY[4]. Even though the SM has helped to understand many things in modern particle physics, the fundamental question about the origin of matter and especially of the masses is still unanswered. The SM is not able to answer this question satisfyingly, therefore the origin of the masses is to be searched in physics *Beyond the Standard Model* (BSM).

One field of research is the *single top quark physics*. It started more than 11 years ago with the discovery of the heaviest quark, the top quark (t), at the Fermilab Tevatron. The fact that the mass of the t quark (∼175 GeV) is of the same order of magnitude as the Electroweak Symmetry Breaking scale (EWSB, ∼250 GeV) makes the top a very interesting object of studies. With the EWSB one expects also new physics to show up, and the top is certainly the most promising candidate for searches toward that direction. The variety of these possible physics Beyond the Standard Model is widely spread: anomalous quark couplings [1], anomalous Wtb couplings [2], new strong dynamics [3], flavour changing neutral currents (FCNC) [4], R-Parity violating SUSY[5] effects [5], CP-violation effects [6], and so on. But all models agree, that the effects should be first visible in the top sector.

The FCNC is the origin for the *Anomalous Top Production* studied here. The FCNC allows a light quark to interact with a neutral gauge boson to form a top quark. Since the SM preserves all flavours in neutral current interactions in leading order, this process is not allowed within the SM.

---

[1] **L**arge **H**adron **C**ollider
[2] **C**onseil **E**uropéen pour la **R**echerche **N**ucléaire
[3] **T**era electron volt **E**nergy **S**uperconducting **L**inear **A**ccelerator
[4] **D**eutsches **E**lektronen-**SY**nchrotron
[5] **SU**per**SY**mmetry

At HERA[6], an exciting experimental fact is the observation of isolated electrons and muons with high transverse momentum along with missing energy and a large hadronic final state [7]. The topology and the kinematics of these events are of a kind that cannot be explained within the SM, but they would fit quite well to the Anomalous Top Production . The present analysis was looking for Anomalous Top Production in the τ-channel, using the data from 1999 - 2000 of H1 with an integrated luminosity of $\mathcal{L} = 62.76$ pb^{-1}.

[6] **H**adron **E**lektron **R**ing**A**nlage

Chapter 2

An Introduction to the Theory

This chapter will give a short introduction to the theoretical aspects encountered in this analysis. The kinematics, the parton model as well as the Anomalous Top Production will be briefly explained. The SM predicts quark flavour conservation in all strong and electromagnetic interactions, therefore the t can only be produced in pairs ($t\bar{t}$). The FCNC 'converts' a lighter quark to a single, or anomalous, t and must be a non-SM process. The decay of the anomalous t is considered to be SM like.

2.1 General Kinematics of ep Reactions

The interaction between electrons and protons (ep)

$$e + p \quad \rightarrow \quad l + X \tag{2.1}$$

is mediated by a gauge boson. The interaction forces are either electromagnetic ($\rightarrow \gamma$) or weak ($\rightarrow W$, Z^0). The gauge boson transfers the (momentum)^2

$$-Q^2 = q^2 = (k - k')^2, \tag{2.2}$$

where k and k' represent the four-vectors $(E, \vec{p})$ of the incoming and outgoing lepton, respectively. Fig. (2.1) shows the corresponding Feynman graph. The outgoing lepton is either an electron (Neutral Current, NC) or a neutrino (Charged Current, CC), and X represents the *Hadronic Final State* (everything else but the lepton).

For $Q^2 \approx 0$ GeV^2 the photons are real, this process is called *Photoproduction* opposed to the *Deep Inelastic Scattering* (DIS) with virtual photons for large Q^2.
In this analysis the entire kinematical Q^2-range was covered.
The two incoming 4-vectors define also the *center of mass energy*

$$\sqrt{s} = \sqrt{(P + k)^2} \overset{*}{\sim} \sqrt{4E_p E_e} \tag{2.3}$$

The last relation ($*$) is valid for storage rings neglecting the masses of the beam particles, electron and proton at HERA. The kinematics of the scattering can be expressed by s and two further independent variables. One possible choice is

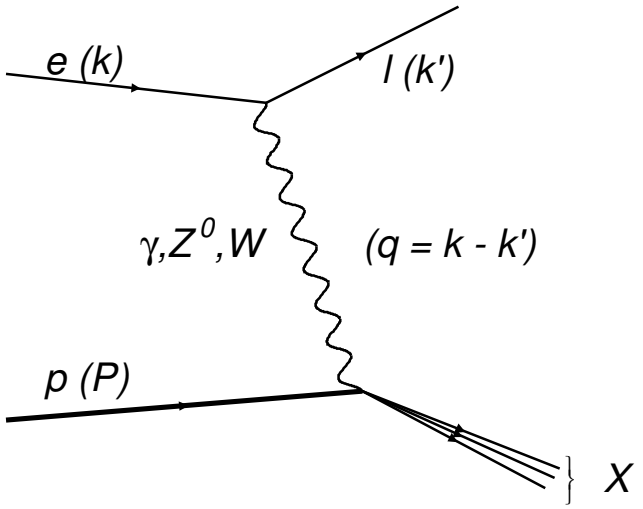

Figure 2.1: The general Feynman graph for ep interactions. The values in brackets stand for the 4-vectors, l is the scattered lepton and X the hadronic final state.

$$x = -\frac{q^2}{2(q \cdot P)} \quad \text{and} \quad y = \frac{q \cdot P}{k \cdot P} \tag{2.4}$$

These variables have the advantage of being dimensionless. x is the *Bjorken variable* and y the momentum transfer by the photon (in proton rest frame). The relation to describe the kinematics is now

$$Q^2 = x \cdot y \cdot s \tag{2.5}$$

Besides x and y, one can also choose Q^2 as independent variable. Historically the second parameter would then be

$$\nu = \frac{P \cdot q}{m_p} \tag{2.6}$$

Q^2 is also a measure for the virtuality of the process ('Is the photon real or virtual?') and ν is the energy of the gauge boson in the proton rest fame.

In the early 1970's, Richard Feynman proposed the *Parton Model* [8], describing the basic constituents of the proton. It explained the phenomenon of the *scaling* [9] described by J. D. Bjorken in 1967.

2.2 Deep Inelastic ep-scattering in the Parton Model

Gell-Mann [10] and Zweig [11] introduced the *Quarks* as constituents of the proton in analogy to the nucleons in the nucleus. The quarks were later recognized as one kind of Feynman's partons, the other kind were the *Gluons*. Each kind of particles carries about 50 % of the proton momentum. The quarks inside the proton are two u 's and one d (valence quarks), and virtual $q\bar{q}$-pairs (sea quarks).
The parton model interprets the deep inelastic ep-scattering as an elastic scattering of the electron off the partons [12]. The electron has to interact by electromagnetic or weak forces with the partons, exchanging a photon or a Z^0-boson (NC) or a W-boson (CC).
The Bjorken variable gets a very descriptive meaning in the infinite momentum frame[1]: It represents the fraction of momentum carried by the parton (see Fig. (2.2)).

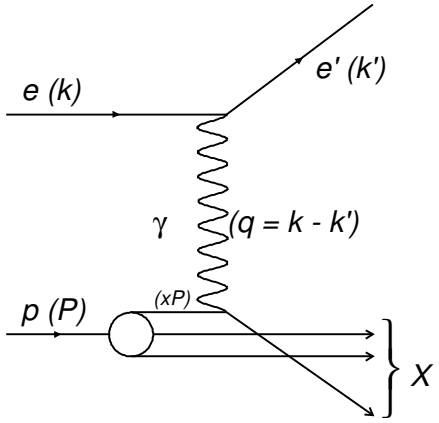

Figure 2.2: Deep inelastic $ep-$scattering as described by the parton model, in brackets the 4-vectors. X is the hadronic final state. The momentum carried by the scattering parton is xP, where x is the Bjorken variable.

Most partons coming from the DIS will hadronize and finally end up as hadrons, a process called *fragmentation*. This fragmentation is not yet fully modeled. It may be described by fragmentation functions of heavy quarks. The most used functional form was suggested by Peterson *et al.* [13]. A heavy parton may either hadronize (e.g.[2] b) or decay in a W (e.g. t) and decay further to leptons and quarks, where the quarks will undergo fragmentation to form hadrons. These hadrons may decay as well (e.g. $\pi^0 \to \gamma\gamma$). All undecayed hadrons together build the *Hadronic Final State* X.
These hadrons may either be isolated or collimated in a narrow group. The collimated hadrons form a so called *Jet*. Jets are mostly the remnants of a single parton (quark or gluon). The reconstruction from the hadrons to the parton is due to the open question during fragmentation very challenging.

[1] A reference frame where the proton carries a large momentum and the transverse momentum of the partons inside the proton is neglectable. In this frame these partons are not interacting with themselves. The laboratory frame at HERA is a valid approximation of the infinite momentum frame.
[2] exempli gratia

2.3 Photoproduction

For low Q^2 the electron scatters off the proton at small angles, exchanging a (quasi)-real-photon. The photoproduction describes a photon-proton scattering process with the electron as photon source.

The hadronic structure of the photon is the origin for several subprocesses contributing to the total photoproduction cross section. These subprocesses can be classified in various ways ([14] and references therein). A photon may split in a $q\bar{q}$-pair (anomalous component) or transform into a vector meson (VDM). These photons are also called *resolved photons*, whereas the photons interacting as point-like gauge bosons (BGF, QCD-Compton) are called *direct photons*. The Feynman graphs for leading order are given in (Fig. (2.3)). This distinction is lost in next to leading order, since higher order effects mix the different processes up.

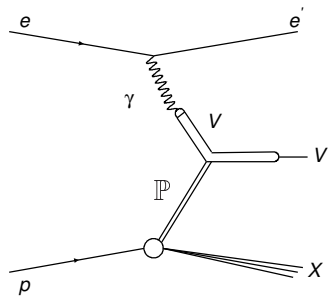

(a) VDM-type resolved

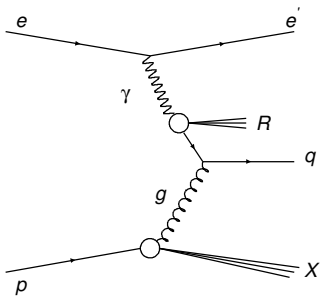

(b) anomalous resolved

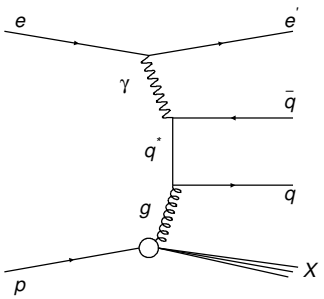

(c) photon-gluon fusion (BGF)

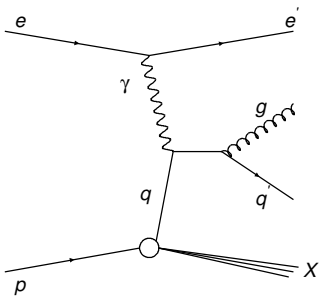

(d) QCD-Compton process

Figure 2.3: Leading order Feynman graph for photoproduction processes. The corresponding process is given below the figure. The V denotes a vector meson ($\rho, \omega, \phi, J/\psi, \Upsilon$) and $\mathbb{P}$ the pomeron.

2.4 Anomalous Top Production and its decay modes

The Anomalous Top Production arises from a *Flavour Changing Neutral Current*. The possible gauge bosons are the γ and the Z^0. For ep collisions the t-channel exchange of a γ is much more likely than the Z^0-exchange [15] since the massive Z^0 is highly suppressed in the propagator compared to the massless γ. Due to the larger parton density in the proton, the coupling to the u-quark is in favor compared to the c-quark coupling (c-quarks are only expected as sea quarks in the proton[3]). For the coupling of the top to the light quarks (u,c) only upper limits from radiative top decays set by the CDF Collaboration [17] are available: $\kappa_{\gamma,u} < 0.28$ [18].

Fig. (2.4) shows the Feynman graphs for the Anomalous Top Production for ep collisions.

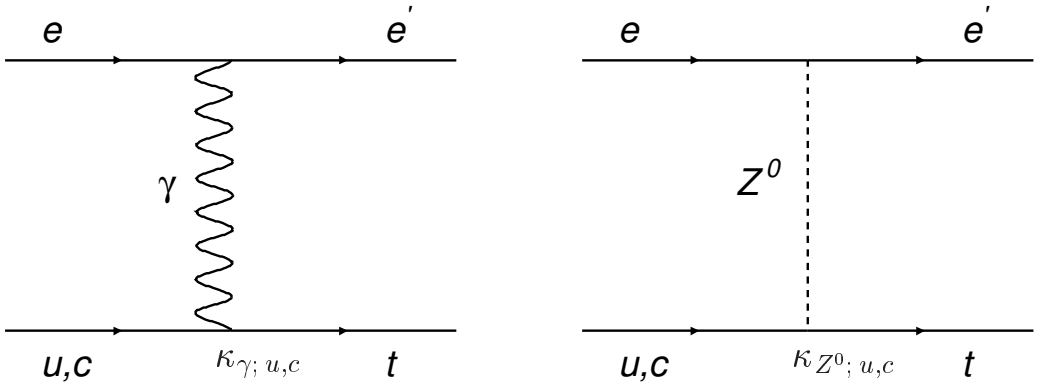

(a) Anomalous Top Production in ep collisions with γ-exchange ...

(b) ... and Z^0-exchange

Figure 2.4: The Feynman graphs for the Anomalous Top Production in leading order for ep collisions. Only the scattering quark from the proton is drawn. Fig. (a) is the relevant process at HERA.

Considering only SM-decays, the top is assumed to decay only into W and b. The b-quark will cause a high energy hadronic jet, whereas the W has several decay channels. The leptonic decays into electron and muon were previously used for searches for Anomalous Top Production at HERA [15]. In this new approach, the third leptonic decay ($W \to \tau\nu_\tau$) was examined. The corresponding Feynman graph is drawn in Fig.(2.5). Since the electromagnetic charge is to be conserved in all interactions, the decay of the top $t \to Wb$ produces only positively charged W bosons and therefore only positively charged τ and π are produced in the top decay chain.

[3]There are hints for an 'intrinsic charm distribution' [16]

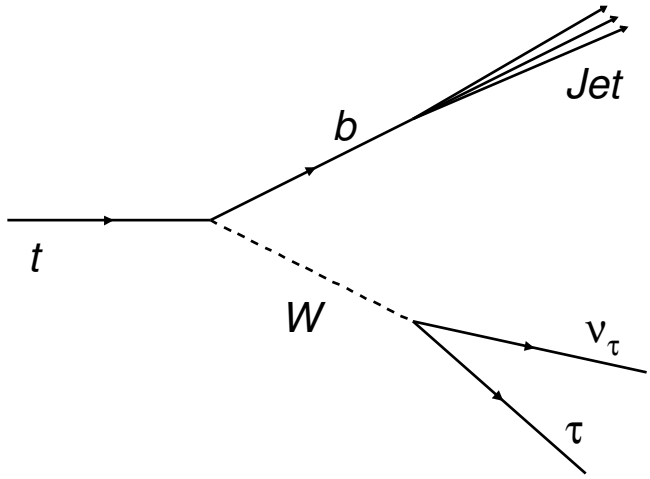

Figure 2.5: The top decay in the τ-channel with missing energy (ν_τ) and a high energy jet (b). The decay $t \to Wb$ separates the space in two hemispheres.

To isolate the Anomalous Top Production, the decay products of the top[4] have to be identified in the detector. The tau lepton decays not only leptonically but also hadronically. The dominant decay is a so-called *hadronic one prong decay*: $\tau^+ \to h^+ + n$ neutrals with a *Branching Ratio* (BR) of 46.7 % [19]. The h^+ stands for a pion or a kaon, where as the pion is much more likely than the kaon. Possible neutral particles are π^0 and neutrinos. Within the one-prong decay the process $\tau \to \pi^+ + n\,\pi^0 + \nu_\tau$ is dominating with a BR of 36 % for $1 \leq n \leq 3$. The main task was to identify the charged pion in the detector. Each neutral pion will decay almost immediately into two photons. The characteristics of the τ decay are the missing energy from the neutrino and one charged track with additional energy in the calorimeter from the γ's. The τ-decay is drawn in Fig.(2.6).

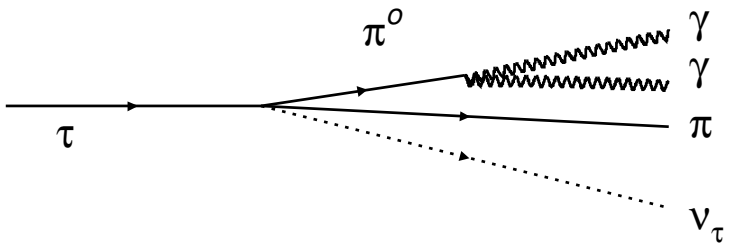

Figure 2.6: The τ-decay: $\tau \to \pi^+\pi^0\nu_\tau$ and $\pi^0 \to \gamma\gamma$.

[4] The expression 'top' refers to the anomalous top (t) as produced in Fig. (2.4(a))

Table (2.1) gives a short summary on the most important particles associated with the decay of the top.

Particles associated with the Top in this Analysis				
Particle	Particle Type	mass [GeV]	Mean Life Time [s]	Considered Decay Mode (BR)
top (t)	quark	174.3	—	Wb (100 %)
W	gauge boson	80.4	$\Gamma = 2.12 \pm 0.05$ GeV	$\tau\nu_\tau$ (10.4 %)
Tau (τ)	lepton	1.78	290.6×10^{-15}	hadronic one-prong (49.5 %)
Pion π^+	meson	0.139	2.6×10^{-8}	no decay
Pion π^0	meson	0.135	8.4×10^{-17}	2γ (98.8 %)

Table 2.1: Summary on all particles associated with the top encountered in this analysis

2.5 *ep* collisions at HERA

This section will give a summary of the possibilities at HERA. A more detailed description of the experimental setup is given in chapter 3.
The dominating process at HERA is the photoproduction. With a center of mass energy of roughly 300 GeV (see chapter 3.1) no $t\bar{t}$-pairs can be produced. So any reported top quarks at HERA would imply a single top physics process.

H. Fritzsch examined the theoretical possibilities of detecting single tops at HERA [20]. With an expected integrated luminosity of about 100 $\text{pb}^{-1}$and favorable circumstances, he predicted the possibilities to find 'a few' events of this type. The isolated leptons reported from H1 Collaboration strongly support the existence of the single top's.

Chapter 3

Experimental Setup

3.1 The HERA Collider

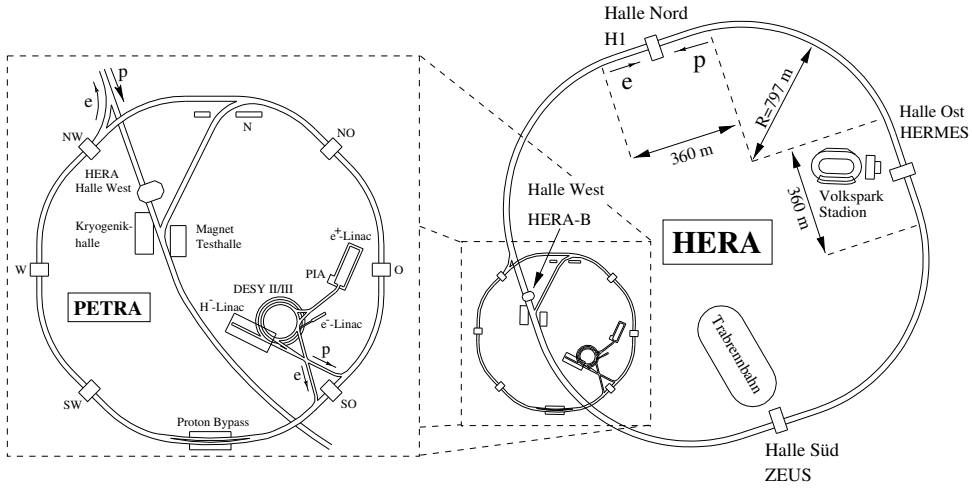

Figure 3.1: The HERA collider with the storage ring and the preaccelerators. The experiment H1 is situated in the northern hall.

At the DESY laboratories in Hamburg, Germany, is the HERA (**H**adron **E**lectron **R**ing**A**nlage). HERA accelerates and stores electrons (or positrons[1]) and protons and provides the unique opportunity to study lepton - quark interactions. The two particle types are gathered in bunches with up to 10^{11} single particles per bunch. During normal operation roughly 220 bunches in 96 ns time intervals circulate in the storage rings representing the electron and proton beams. The two storage rings are 6.3 km long and are roughly 20 m below the surface. For the proton ring superconducting magnets have to be used to bend the proton beam to a stable trajectory.

[1]most runs at H1 were made using positrons (e^+) instead of electrons (e^-), from now on 'electron' refers to both particles.

Since 1992 the electrons and protons are preaccelerated with various linear accelerators (LINAC) and two former storage rings (DESY, PETRA) and then fed to the large HERA rings where the particles will reach their final energies of 27.6 GeV and 820 GeV, respectively, leading to a center of mass energy of $\sqrt{s} = 301$ GeV in the collision (see equation 2.3). Since 1999, the protons are even accelerated to 920 GeV pushing the center of mass energy to $\sqrt{s} = 319$ GeV. An overview of the preaccelerators and the HERA rings is given in Fig. (3.1).

Along the storage rings of HERA are 4 large experimental halls. In the northern hall is the experiment H1, an international collaboration of about 400 scientists from 39 institutes of 12 countries throughout the world. Here the electron and proton beams are collided head-on. The resulting particles of the collisions are detected with the general purpose H1 detector. The main interest of research of the H1 collaboration is to measure the structure of the proton, to study the fundamental interactions between particles, and to search for physics Beyond the Standard Model of the elementary particles. The three other halls are occupied by the experiments HERMES, ZEUS and HERA-B.

3.2 H1 Detector

Unlike most other High Energy Physics Detectors, the H1 Detector is not symmetric with respect to the nominal interaction point[2]; this is due to the different energies of the two beam particles. The proton has more energy (momentum) than the electron and the greater momentum along the beam axis causes the main event to be shifted in flight direction of the proton beam. This also defines the *reference frame* at H1: The positive z axis is along the proton beam and is called the forward direction, perpendicular to it is the xy plane (where the x-axis points toward the center of the ring and the y-axis points upward). It is also referred to as the *transverse plane*. The origin of the coordinate system is defined as the nominal interaction point.
There are further two angles of importance: θ and ϕ: θ is the *polar angle* between the trajectory and the z-axis (scattering angle), ϕ the *azimuthal angle* in the transverse plane with $\phi = 0$ corresponding to the positive x-axis. For lorentz invariance one introduced the variable *rapidity* $\hat{y}$. In most cases the relevant parameter is the *pseudo-rapidity* η which is an approximation of $\hat{y}$, neglecting the masses of the particles ($m = 0$). The pseudo-rapidity is correlated with the polar angle θ

$$\eta = -\ln\left(\tan\frac{\theta}{2}\right) \tag{3.1}$$

η and ϕ assure a set of coordinates, where the difference in each coordinate is lorentz invariant.

Fig. (3.2) shows the H1 detector with the reference frame and the asymmetric structure.

[2] The nominal interaction point is the point where the electron and proton beams collide.

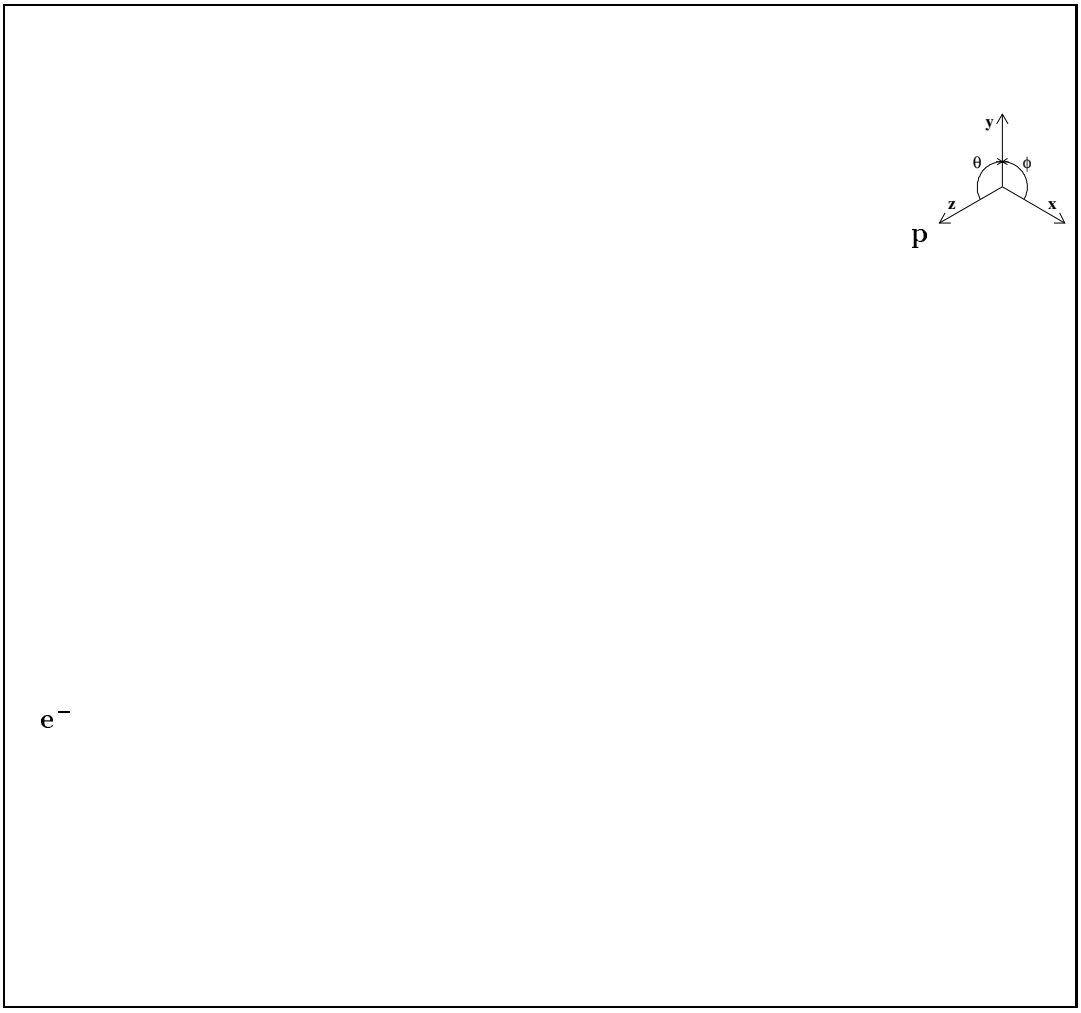

1	Beam pipe and beam magnets	9	Muon chambers
2	Central tracking device	10	Instrumented iron yoke
3	Forward tracking device	11	Forward muon toroid
4	Electromagnetic LAr calorimeter	12	Backw. electromagn. calorimeter (BEMC)
5	Hadronic LAr calorimeter	13	PLUG calorimeter
6	Superconducting coil (1.15 T)	14	Concrete shielding
7	Compensating magnet	15	Liquid argon cryostat
8	Helium supply for 7		

Figure 3.2: The H1 Detector [21]. The asymmetry in proton flight direction is clearly visible.

This asymmetry in the polar angle θ splits the H1 detector in three major regions listed in table (3.1). The present analysis only considers particles in the central region.

Angular Regions of the H1 Detector	
Region	Angular coverage
forward	$7^\circ < \theta < 25^\circ$
central	$25^\circ < \theta < 155^\circ$
backward	$155^\circ < \theta < 175^\circ$

Table 3.1: The three angular regions of the H1 detector, for the polar angle θ. $\theta = 0^\circ$ is the proton beam flight direction.

A detailed description of the H1 detector is available in [21]. The important elements of the detector are shortly summarized.

3.2.1 Tracking Chamber

Consisting of Drift chambers, this part is responsible for measuring the trajectories of the charged particles and the vertex[3] information. A charged particle penetrating the tracking chamber will leave a trace in the chamber, this trace describes the trajectory of the particle and is generally called *track*. According to the three angular regions, are three tracking devices implemented: *Forward Tracking Detector* (FTD), *Central Tracking Detector* (CTD) and the *Backward Drift Chamber* (BDC).

Fig. (3.3) shows the H1 tracking system in r-z view. One can clearly see the three different angular regions from table (3.1).The CTD is based on two concentric drift chambers, the *Central Jet Chambers* CJC1 and CJC2 (See Fig. (3.4)), and the two z-vertex chambers CIZ and COZ (inner and outer, respectively).

The tracks are described by five kinematical parameters = ($\varkappa$, ϑ, φ, d, z). The physically relevant parameter is the transverse momentum. It is measured with a magnetic field (1.2 Tesla) provided by the superconducting coil (chapter 3.2.3). The momentum will be calculated by the equation

$$P\cos(\lambda) = 0.3 \cdot z \cdot B \cdot R. \tag{3.2}$$

The trajectory of a particle with momentum p (in GeV/c) and electric charge ze in a constant magnetic field $\vec{B}$ is a helix with curvature R (in meter) and pitch angle λ. At H1 the empiric equation for the transverse momentum is

$$P_T[GeV] = 0.345 \cdot R. \tag{3.3}$$

[3] the vertex is the real interaction point

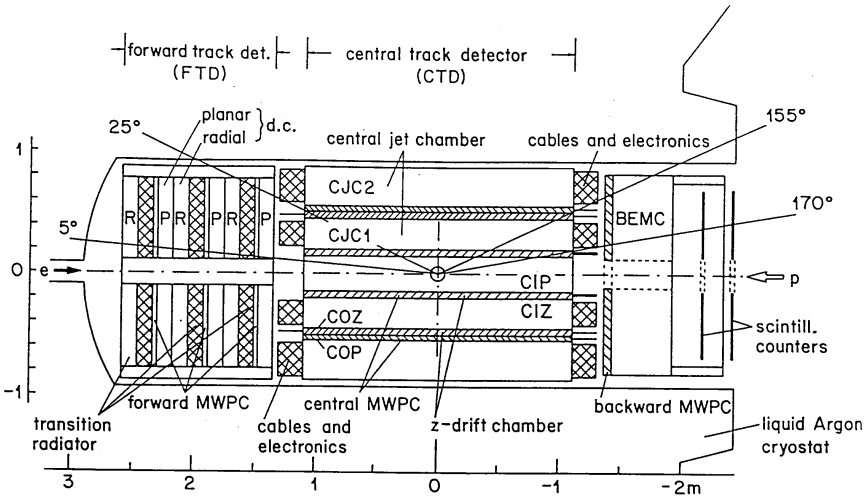

Figure 3.3: The H1 Tracking system in r-z view. Note that the BEMC was replaced by the SpaCal and the MWPC by the BDC.

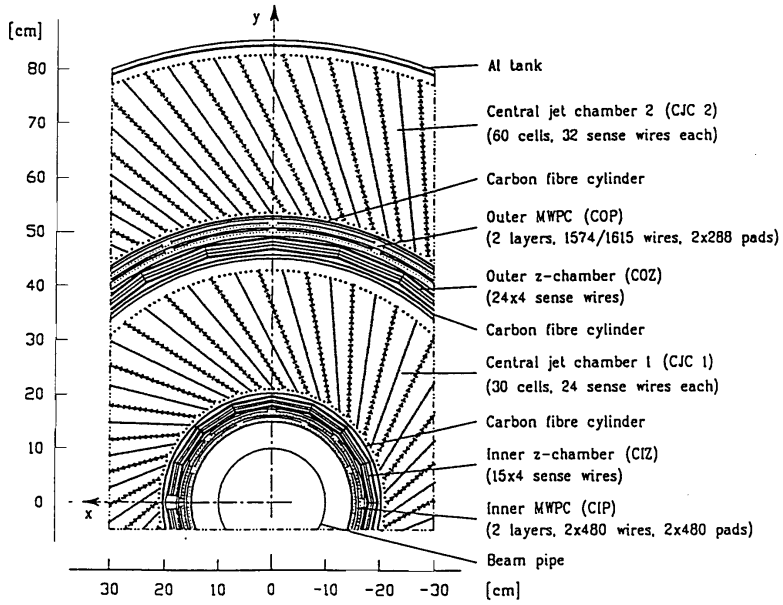

Figure 3.4: An r-ϕ view of the central jet chambers CJC1 and CJC2

The determination of the curvature R is based on the signals recorded from the CJC1 and CJC2 devices and is correlated to $\varkappa$ by

$$R \sim \frac{1}{\varkappa}. \tag{3.4}$$

3.2.2 Liquid Argon Calorimeter (LAr)

In the central region of the detector only one Calorimeter is needed, the *Liquid Argon*. It covers an angular range from $4° < \theta < 153°$ and is divided in an electromagnetic (ECAL) and a hadronic (HCAL) part. They measure the energies of electrons, photons and hadrons by absorption. The charged particles and the photons will shower up in the corresponding calorimeter and deposit their energy. Muons will deposit an equal amount of energy in both parts of the LAr by ionization. The precision of the measured energy for electromagnetic showers is $\sigma(E)/E = 12\%/\sqrt{E/GeV} \oplus 1\%$ and for hadronic showers $\sigma(E)/E = 50\%/\sqrt{E/GeV} \oplus 2\%$ [22].

Fig. (3.5) shows the individual parts and the segmentation of ECAL and HCAL. One can clearly detect the central (CB 1 - 3) and the forward barrels (FB 1 - 2, IF, OF) as well as the distinction between the ECAL and the HCAL sections.

The LAr is highly segmented in cells. These cells collect the charges from the ionization and the showers. The calorimeter reconstruction program converts the charges to energies in the calorimeter cells for electromagnetic and hadronic showers. Each cell passing the cell level reconstruction is subject to clustering. The cluster algorithms are tuned so that the cells containing energy depositions from electromagnetic showers are most probably merged into one cluster whereas for the hadronic showers the energy depositions are split into several clusters.

Another important difference between the ECAL and the HCAL is the electromagnetic scale. Hadrons deposit roughly 30 % less electromagnetic energy than electrons and photons. The LAr is not compensating this difference, therefore two different *energy scales* are used in the reconstruction:

- The 0-level contains the raw measured electromagnetic energy in the Calorimeter.
- The 1-level has been corrected for dead material.
- The F-level applies a special compensation factor to all hadronic particles distinguishing between the electron scale and the hadron scale.
  Note: the energy for reconstructed muon-candidates get the same compensation factor as well, since the muons pass through the HCAL.

This compensation factor is achieved by a different calibration used for the conversion from measured electromagnetic energy (0-level) to the final energy (F-level).

Further Calorimeters are part of the detector for complementation in backward (BEMC,SpaCal) and forward (PLUG) direction.

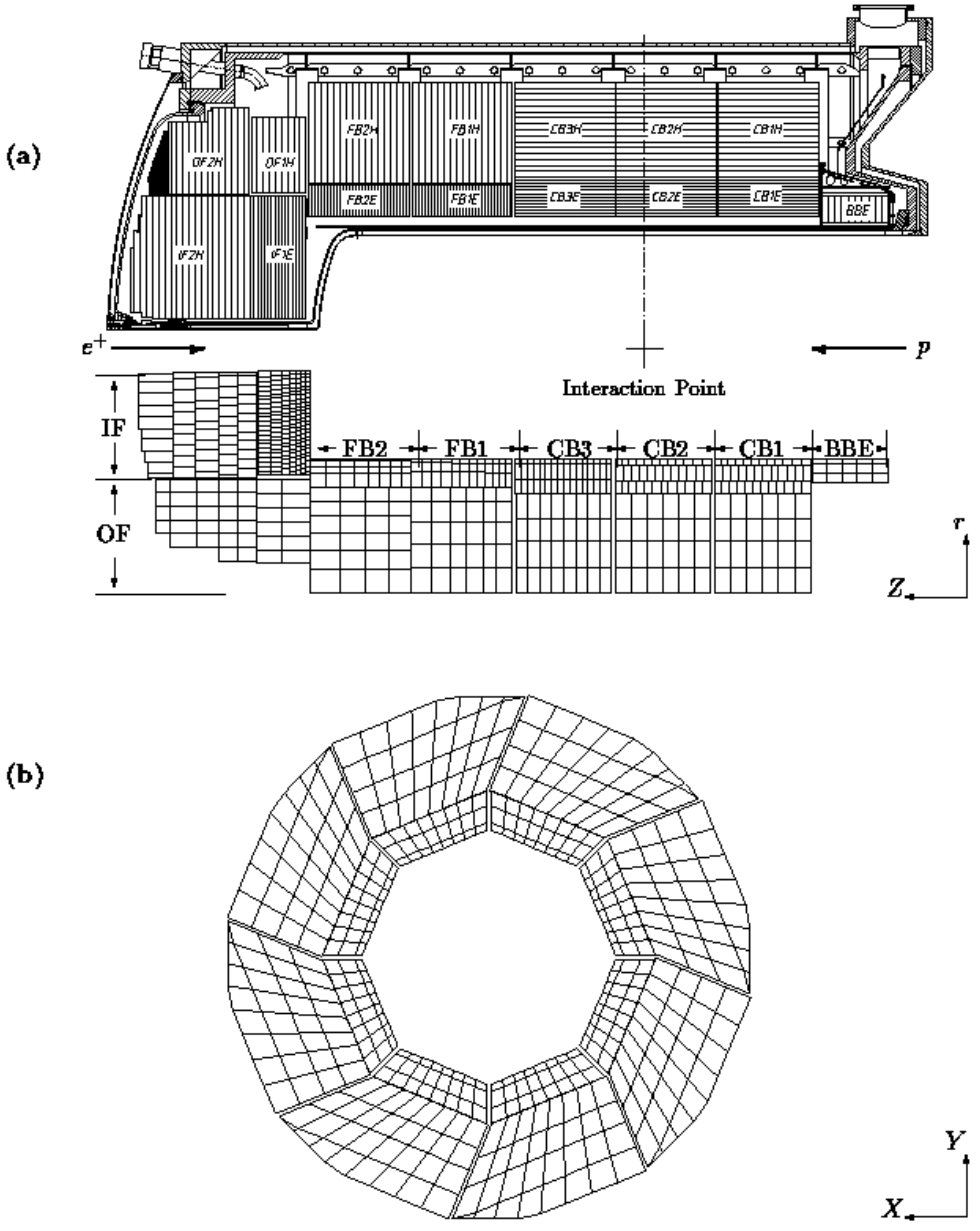

Figure 3.5: LAr calorimeter in r-z view (a) showing the division into individual parts and the orientation of the absorber layers and the cell segmentation (b) in r-ϕ view. The ending 'E' stands for the ECAL and 'H' for the HCAL. One can clearly see the partitioning of the LAr calorimeter in central barrels (CB 1 - 3) and forward barrels (FB 1 - 2, IF, OF).

3.2.3 Superconducting Coil and Iron Yoke

The solenoid provides a magnetic field of 1.2 Tesla, parallel to the z-axis and bends the track for the determination of the transverse momentum in the xy-plane. It is further helpful to distinguish between neutral and charged particles (e.g. electrons and photons).

The iron yoke is instrumented with streamer tubes, and measures the leakage of hadronic showers outside the Calorimeter (Tail Catcher). The hit pattern in the streamer tubes together with the muon system allow to reconstruct particle tracks penetrating the detector (muons).

3.2.4 Trigger System and Reconstruction

The collision rate at the interaction point is roughly 10 MHz, but the band width for the recording is limited to 10 Hz. Quite logically it is not possible to store all collision events to tape for later analysis, but rather a small sample of selected events. To determine which events are to be kept and which ones can be rejected, the *Trigger System* was developed. The entire trigger system is set up in 4 Levels.

- The first level (L1) has 2 μs to decide whether the event is passed on to the second level (L2) or already rejected at L1. The decision is based on several signals from the subdetectors totaling in 256 subtrigger elements. Subtrigger elements are mostly thresholds which have to be exceeded to set the corresponding subtrigger. A subtrigger is a single subtrigger element or a combination of them. The subtrigger elements are combined to 128 subtriggers.
  A rejection may also occur due to a prescaling of the subtrigger. The prescale is an internal counter set to n, rejecting the first $n-1$ events, keeping the n^{th} event, rejecting the following $n-1$ and so on. The counter usually counts for each subtrigger element individually.
  The trigger condition for interactions with high transverse energy is derived from the signals of the LAr.

- After passing the L1, the second level (L2) is started. Simultaneously the readout of the entire subdetector information is initiated. The L2 provides another 16 subtrigger elements. The readout of the subdetectors takes some 1-2 ms and compared to the collision rate of 96 ns between a collision far too long. Therefore L2 requires after 20 μs a validation of the L1 decision, using the new subtrigger element information and the combined information from L1; otherwise the readout is stopped and reset.

- The third level (L3) is not implemented. Its purpose is to make another validation after a few 100 μs. This would cause a further reduction of the input rate for the next level.

- The fourth level (L4) is purely software based and has access to all subdetector information. This level is not integrated in the detector, but rather hosted by a processor farm performing a partial event reconstruction. Its algorithms are tuned to select well known physical processes as well as reject background processes, mainly from beam-gas or beam-wall interactions. This level is independent from the collision rate (asynchronous) since the full readout is stored in a data pipe.

The full reconstruction of the event is done after passing L4. The L4 raw data is processed by *H1REC* the reconstruction software used at H1 on a dedicated multiprocessor workstation (sometimes referred to as L5). The final events are classified as candidates for selected physics processes and written to *Production Output Tape* (POT). A shorter version is written to *Data Summary Tape* (DST), which is sufficient for most analysis. The present analysis was made using the DST tape information.

For the present analysis two subtriggers were required, they are called ST67 and ST77 (Subtrigger 67 and 77). Both subtriggers were used to trigger muonic W decays [23]. The top decay has similar topological and kinematical characteristics, so these subtriggers will work for the present analysis as well. The specifications and subtrigger elements are given below.

- Subtrigger ST67

  `s67  LAr_electron_1`

  The subtrigger element *LAr electron 1* is set, if the energy in one trigger tower[4] exceeds the threshold of 6 GeV for L1. No prescale is needed ($n = 1$).

- Subtrigger ST77

  `s77  LAr_Etmiss>1`

  The subtrigger element *LAr Etmiss* describes the imbalance of transverse momentum measured in the LAr. As in ST67 there is also no prescale needed.

The trigger efficency for the two triggers combined is $99\%^{+1}_{-0}$ within the visible kinematic region of the present analysis [24].

[4] A group of neighboring cells

3.3 Luminosity System

The determination of the *Integrated Luminosity* ($\mathcal{L}$) is necessary for the calculation of cross sections. For this purpose the Bethe-Heitler-Process $ep \to ep\gamma$ is used, a well known QED[5] process. The detection of the scattered electron and the photon takes place in two Čerenkov-detectors, the *Electron Tagger* (ET) and the *Photon Detector* (PD) located at 33.4 m and 102.9 m, respectively up the proton beam (negative z-axis).

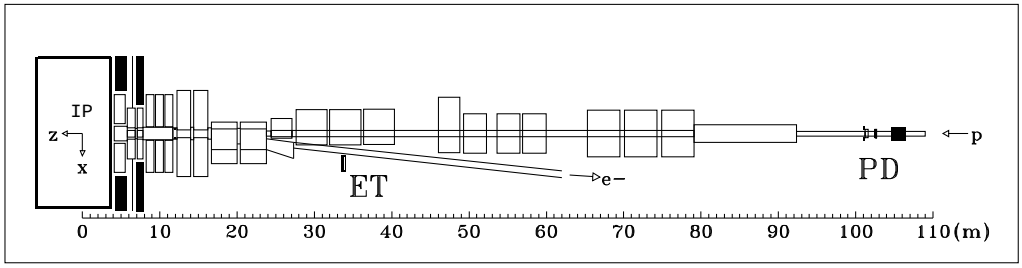

Figure 3.6: The Luminosity system of H1. The H1 detector is on the left. The scale is along the negative z-axis starting at the nominal interaction point ($z = 0$).

The measured luminosity has to be corrected twice:

1. Beam-gas interaction
   In the beam pipe is always some rest gas left (no perfect vacuum possible). The electron bunches also interact with this gas contributing to the luminosity, but not to the data (outside the detector acceptance). Therefore some pilot bunches, electron bunches with no proton counter bunch and hence only interacting with the rest gas, are put in between the electron bunches colliding with proton bunches, to determine the contribution from the beam-gas interaction to the luminosity.

2. Analysis correction
   A malfunction of one of the subdetectors or any other reason causes some data information to be lost. The data taken during the time period of such losses is to be excluded from the analysis. Also single events or runs may lack some required information. By excluding all these runs, the luminosity for these runs is also to be subtracted.

In the end the integrated luminosity for the data 1999 - 2000 added up to

$$\mathcal{L}_{\text{tot}} = \int \mathcal{L}_{\text{run}} \mathrm{d}t = (62.76 \pm 0.94) \quad pb^{-1} \tag{3.5}$$

[5] **Q**uantum **E**lectro**D**ynamics

Chapter 4

Monte Carlo and Background

Monte Carlo (MC) is a software based method of simulating different physical processes. It consists of two major parts: The *Monte Carlo Generator* generates on parton level the 4-vectors of the particles according the the SM and relativistic kinematics, and in a second step, the *Monte Carlo Simulator* (*H1SIM, GEANT*) simulates the subdetector information from the generated 4-vectors. The output of the Monte Carlo Simulator is used as input for the reconstruction mechanism (H1REC,L5) of the detector. This assures that the generated processes undergo the identical reconstruction and analysis chain as the actual data. These reconstructed events are stored in *Monte Carlo files*.

4.1 Anomalous Top Production Monte Carlo

For the Anomalous Top Production several Monte Carlo files are available. The Monte Carlo Generator *SUSYGEN* [25] was designed to generate events from BSM, especially SUSY. The generated events for the Anomalous Top Production assumed 27.5 GeV and 920 GeV for the electron and proton energy, respectively. For the decay chain, only the decays $t \to Wb, W \to \tau\nu_\tau$ and the hadronic decay channels of the τ were generated. These hadronic τ decays have a total BR of 64.8 %.

The Monte Carlo file contains 25'000 simulated events. Since there is no coupling $\kappa_{\gamma,u}$ measured, a luminosity can not be given. Fig. (4.1) shows an example of a simulated Anomalous Top Production event from the Monte Carlo files.

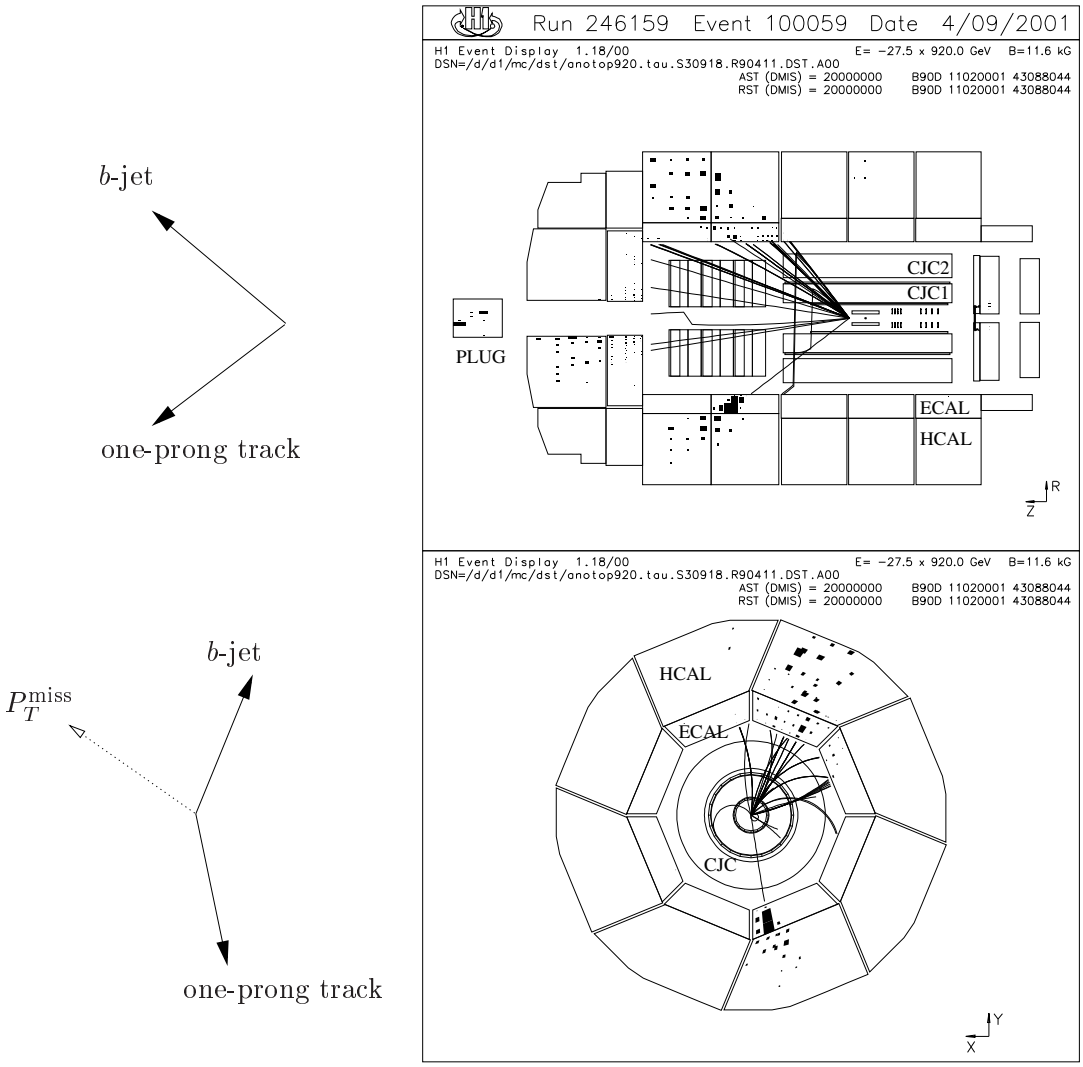

Figure 4.1: A simulated Anomalous Top Production event generated by the Monte Carlo Generator SUSYGEN. To the left of the display is the schematic layout of the event drawn. The upper part of the display shows the reconstructed event in the H1 detector in r-z view. The four inner rectangles represent the tracking chamber (CJC1 and CJC2 from Fig. 3.3) and the two outer layers correspond to the LAr calorimeter (ECAL and HCAL from Fig. 3.5). The trajectories of the particles are drawn as lines originating from the actual event vertex. Clearly visible is the isolated track corresponding to the τ remnant as well as the tracks to the left corresponding to the b-jet. The dark boxes inside the calorimeter represent the energy depositions in the corresponding calorimeter part.
The lower part of the display is in r-ϕ view of the same event showing only the central region of the upper image. The b-jet is only visible in the tracking chamber (inner circles, CJC1 and CJC2) since the energy deposits of the jet is in the forward detector. The τ remnant is clearly visible as energy deposition in the ECAL (inner squares) and the HCAL (outer squares) and can be interpreted as one prong charged pion or kaon.

4.2 Background

The top decay has a very clear experimental signature. But there are other processes with a significantly higher cross section that may fake this signature. Since the analysis focuses on the leptonic decay of the W, the dominant background comes from *SM W Production*. Further background processes within the SM are coming from *Lepton Pair Production* and *Jet Photoproduction* as well as *non-ep Background*.

4.2.1 Non ep Background

There are two sources beside the ep collisions that have to be considered

1. Beam-gas and beam-wall interactions
   The particles in the beam also interact with the rest gas in the beam pipe and the wall of the vacuum pipe. If these interactions occur close by the detector, the remnants of the interactions may enter the detector. Most of the time the triggers will reject these events, since they occur in absence of a bunch crossing.
   The H1 collaboration has developed algorithms [26] looking for non-ep background triggering in the detector (see chapter 3.2.4).

2. Cosmics
   The atmosphere of our planet gets hit several million times a second by high energetic particles from space. These particles initiate huge air showers. The muons, having a long lifetime, reach the surface of the earth and may hit the detector. The topology of these cosmic muons is very clear: A single high energetic track penetrating the entire detector. If the muon 'showers' in the detector, it leaves a single track and a large energy cluster on the opposite side.
   Again the rejection routines from [26] work quite well, but there are still a few events triggering. The topology of a single track, large energy (even large missing transverse energy if the muon only passes parts of the detector) makes this background compatible with the signal for the present analysis. Two cosmic events encountered in the analysis are attached in Appendix A.

4.2.2 SM W Production (γp)

All SM W production processes are contributing to the background. Since the W from Anomalous Top Production originates from a top decay it is boosted, whereas the SM W is more or less in rest. This makes the resulting particles from a top decay more energetic and will enable a hard P_T^{track} cut.

The Monte Carlo generator used for the SM W production is the EPVEC [27] Generator, considering the decays

$$ep \to e'WX \to e'(\tau\nu_\tau)X \quad \text{and} \quad ep \to e'WX \to e'(\mu\nu_\mu)X. \tag{4.1}$$

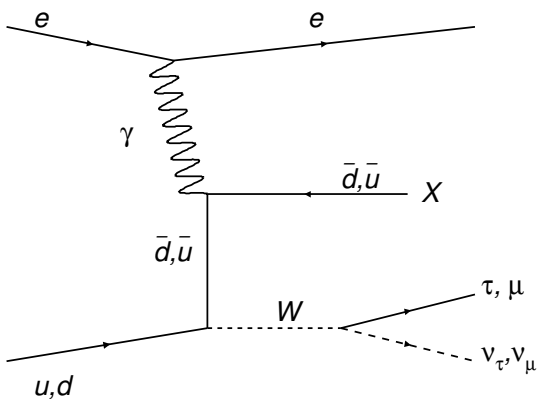

Figure 4.2: γp reaction producing a SM W. This background is generated by the EPVEC Generator. The hadronic final state X arises by fragmentation of the single parton $(\bar{d}, \bar{u})$.

4.2.3 Lepton Pair Production ($\gamma\gamma$)

The background from $\gamma\gamma$- interactions results in lepton pair production, see Fig. (4.3). For a $\tau\bar{\tau}$-pair the missing transverse energy is determined by two neutrinos as well. The big difference to the signal is the high energetic π^+ from the τ decay. The τ from lepton pair production is less energetic than the one from a W decay.

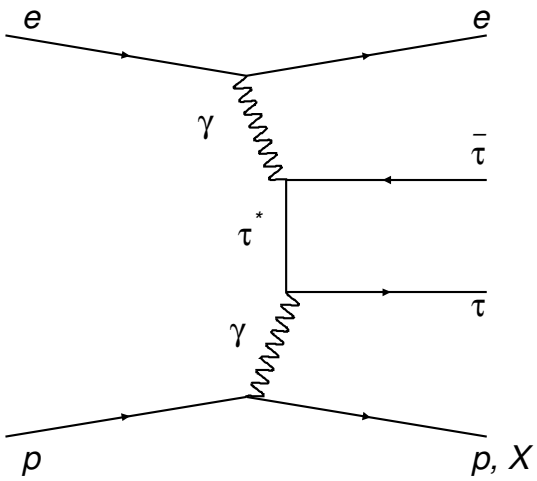

Figure 4.3: Lepton pair production in $\gamma\gamma$ interaction as generated with the LPAIR Generator.

The generator used for this background is the LPAIR [28] Generator.

4.2.4 Standard Model Jets (γp) and Single π-Jets

Usually jets coming from a quark have a very high multiplicity[1]. But if for some reason a low multiplicity jet looses some tracks in dead material or cracks, the detector may see a one-prong jet. Another source for one-prong jets is the scattered electron or single charged pions. The PYTHIA [29] Generator simulates SM jets with $P_T^{\text{track}} > 3.5$ GeV and $|\eta| < 4$.

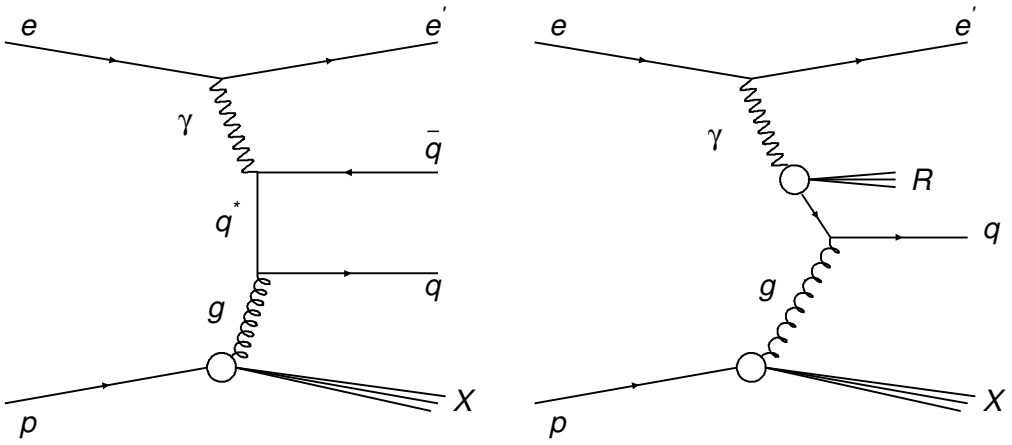

(a) γp interaction with direct photons (BGF) ...

(b) ... and resolved photons (anomalous)

Figure 4.4: Leading order Feynman graph for photoproduction as generated by the PYTHIA Generator.

The Feynman graph for direct photons (Fig. (4.4(a))) looks very much like the lepton pair production (See Fig. (4.3)), only the γ interacting with the proton is replaced by a gluon. The switch to the strong interaction instead the electromagnetic increases the cross section.

4.2.5 Anomolous top decay in muons

The BR for the W decaying into the τ is identical to the BR for the muonic process: $W \to \mu\nu_\mu$. Therefore the top decay

$$t \to Wb\,, \quad W \to \mu\nu_\mu \tag{4.2}$$

is as possible as the signal. The event topology and especially the kinematics of these events look very much like the signal. The analysis has rejected electrons but not muons, therefore the muonic process is also to be considered in the background for the decay into the τ channel.

[1] The multiplicity is the number of tracks in the jet.

The muonic process is simulated in an identical manner as the tau decay. The background will only be given as a ratio between the decay into tau and the decay into muons, since there is no integrated luminosity for BSM processes available.

Several cuts are applied to isolate the signal from all background processes. The cuts and procedures are explained in detail in chapter 5.

Chapter 5

Event Selection

In the years 1999 - 2000 the H1 experiment stored approximately 100 Million events on tape. For this analysis the following data were used:

- 1999: positron - proton collisions
  Run range: 244968 - 259270 / 259281 - 259461
- 2000: positron - proton collisions
  Run range: 262144 - 278686 / 278979 - 279215
  Note: The shifted vertex run was excluded

Within these 100 Million events are only a few single top events expected within the model described in chapter 2.4. The isolation of these events is achieved with rather hard kinematical cuts. This chapter will give an introduction to the methods of the isolation and define the necessary kinematical cuts to isolate the Anomalous Top Production.

5.1 Principle of the analysis

To find a rare process within millions of events, one has to search very particularly. The analysis of the desired process is done using the simulated events from the Monte Carlo files (See chapter 4.1). The optimization of the selection process and background rejection is based on MC simulation of the Anomalous Top Production process. Once the optimization is satisfying the cuts are performed on the data.

For the Anomalous Top Production decaying into a τ, the most significant topology is a one-prong jet with high P_T^{track} and large P_T^{miss} (See Chapter 2 and 5.2). A jet algorithm was used to reconstruct the τ (see chapter 5.3). The characteristics of this decay is one charged particle and additional energy (see chapter 2.4). The most obvious character of the top decay chain topology is large missing transverse energy. These facts are used for a preselection, where all events with a possible Anomalous Top Production topology are selected (chapter 5.5). These candidate events will be subject of a more detailed study with more kinematical restrictions.

The kinematical requirements are divided in two groups:

1. Event variables
   These are variables concerning the entire event, such as P_T^{miss}.

2. Jet variables
   All other variables are correlated with the one-prong jet and characterize its kinematic and topology.

A detailed list of all kinematical variables is given in chapter 5.4.

5.2 Reconstruction of the Event

Due to fragmentation the reconstruction is quite difficult. The decay chain is

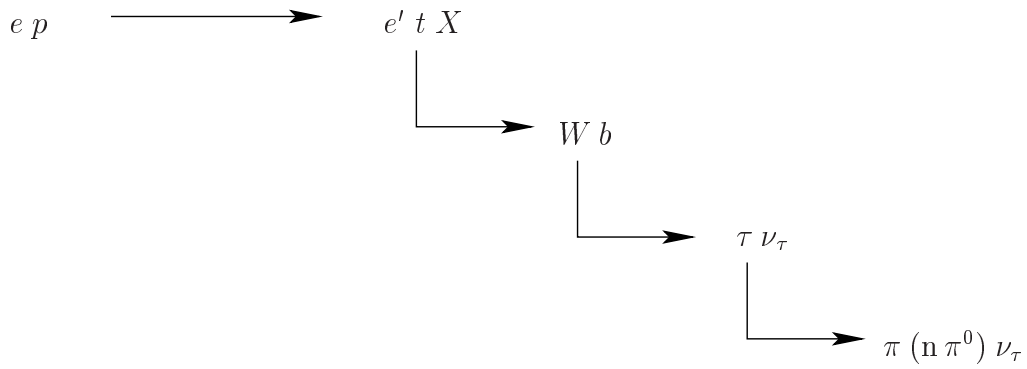

Figure 5.1: The full decay chain considered in the present analysis.

The reconstruction of the top requires a full reconstruction of the W and b. The b hadronizes and produces a hadronic jet, the leptonic W decay contains a neutrino. Neutrino reconstruction is based on the missing transverse energy in the detector, which is defined as the neutrino's transverse energy (momentum). The leptonic decay of the τ produces a second neutrino. The total missing transverse energy in the detector is the sum of these two neutrinos, and it is impossible to reconstruct the energy of either one of the neutrinos. Therefore a full reconstruction of the W is not possible and the t won't be reconstructed completely either.

A detailed study of the kinematics and topology of the detectable particles is necessary. The two neutrinos carry quite a large momentum and therefore the large missing energy is a characteristic topology of the event. Further characteristics are found within the τ decay: Originating from a high energetic W, the τ is expected to have a large momentum as well. The decay topology of the τ can be interpreted as a jet with only one track (one-prong jet). This interpretation was the basic idea for the τ identification. The jet is expected to be very narrow, since the τ is boosted in flight direction of the W. Considering the fact, that the W-boson was boosted itself, the resulting decay particles are more energetic than

particles resulting from a SM W-decay.

The entire event topology is characterized by:

- Two jets, not back-to-back.
- One jet is one-prong with a high energetic particle resulting from the W-decay. The boost in flight direction of the τ makes the one-prong jet rather narrow.
- The particle from the one-prong jet carries a positive electromagnetic charge.
- Large P_T^{miss}, due to two leptonic decays with a neutrino in each decay.
- The decay of the top separates the space in two hemisphere ($\eta\phi$-space). Therefore the one-prong particle is isolated.

5.3 The Jet Algorithm *QJCONE*

5.3.1 Definition of the Jet

The analysis was made completely using *H1PHAN* software. The Hadronic Final State (HADFS) is stored in a class as *Combined Objects* [30]. The combined objects contain tracks and clusters. These combined objects are used by the jet algorithm *QJCONE* [31] to reconstruct the jet.

H1PHAN only considers 'good' tracks, that are tracks passing a certain quality cut. These cuts are implemented in the track selection code for H1PHAN [32]. For the track selection in the present analysis, the steering from the Heavy Flavour Group at H1 was used. The settings for central tracks are given below (from the QHQT bank in [32]):

```
==========CENTRAL CUT DEFINITIONS=========
Minimum Pt in GeV/c        :  0.150000006
Minimum Theta in degrees   :  20.
Maximum Theta in degrees   :  160.
Maximum |DCA| in cm        :  2.
Maximum RSTART in cm       :  50.
Angle for track length cut :  150.
Minimum track length in cm (theta<angle) :  10.
Minimum track length in cm (theta>angle) :  5.
Double track RPTPHTH value :  1.
Minimum number of CJC hits :  0.
```

Explanation to the different variables used for the track selection:

- P_t and $Theta$ (θ) are the transverse momentum and the scattering angle, respectively.
- The $|DCA|$ is the corrected Distance of Closest Approach to the actual event vertex position and not the default $(0, 0)$.

- $RSTART$ expresses the radius of the start of the track.
- $TrackLength$ is the difference between the radius at the end of the track and that at the start, it is calculated in the xy plane.
- And $RPTPHTH$ is the variable used for double track removal.
- $CJChits$ stands for the number of signals received from the CJC1 and CJC2 devices in the tracking chamber (chapter 3.2.1).

A detailed description of these selection cuts is available in [32].

Two further steering banks are of importance: $QHSC$ is the steering bank for the definition of the HADFS, and $QCOMB$ is the steering for the combined objects.

These combined objects include tracks and clusters, therefore the energy of the charged particles are counted twice: once as track and once in the calorimeter as cluster(s). To avoid the double counting, the energy of the tracks is rescaled. All tracks with an energy of more than 350 MeV will be scaled down to 350 MeV. This is the approximate energy loss of a charged particle by passing through dead material and the tracking chamber.

The forming of the jets is controlled by QJCONE; the relevant parameters are listed below.

- Initiator energy
  The minimum energy requirement for an object to be taken as seed for the jet. The seed will be the center of the jet.
- Jet energy
  The summed energy of all jet objects has to exceed this threshold.
- Jet radius
  The opening angle of the jet is measured in $\eta\phi$-space and is defined as $R = \sqrt{\Delta\eta^2 + \Delta\phi^2}$, where the Δ refers to the seed of the jet. The geometrical form of the jet is a conus shown in Fig. (5.2).

The settings of the steering parameters are given in table (5.1).

Settings for Jet Algorithm Steering	
Parameter	Value
Initiator energy	2 GeV
Jet energy	6 GeV
Jet radius	1

Table 5.1: The jet algorithm was run with these parameter settings

5.3.2 Reconstruction of the τ Jet

Fig. (5.2) shows the schematic decay of the τ with the jet radius R. Notice that the single track is not necessarily the seed and therefore it doesn't have be in the center of the jet.

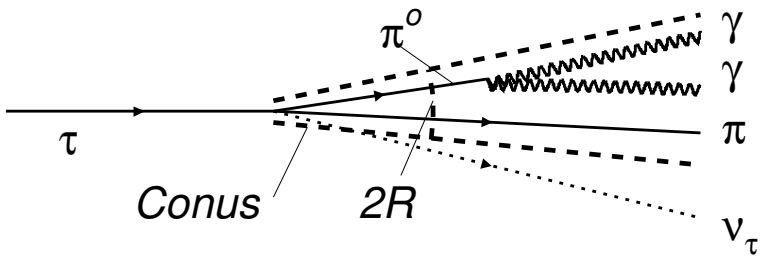

Figure 5.2: The schematic layout of the jet and the conus.

The jet algorithm loops over all combined objects to find an entry which fulfills the initiator energy criteria. This entry will be taken as seed for the jet. Once the seed is set, the algorithm takes all entries within the jet radius and adds them to the jet. If the sum of the energies of all entries exceeds the jet energy threshold, all contributing entries are stored as a jet in a user defined class. This class is also the basis for the calculation of the jet axis or *Thrust* $\vec{T}$.

5.4 Sensitive kinematical variables for Anomalous Top Production

The selection procedure is based on methods developed for charged current (CC) analysis [33] as well as previous Anomalous Top Production searches [7]. The variables used to quantify the event kinematics are listed below:

- P_T^{track}
  The transverse momentum of the track in the one-prong jet. The entire momentum vector is defined as

$$P = \left(\begin{pmatrix} P_x \\ P_y \end{pmatrix} \right) = \begin{pmatrix} P_T \\ P_z \end{pmatrix} \tag{5.1}$$

  P_x is the x-component of P_T, P_y the y-component. P_T^{track} is defined as

$$P_T^{\text{Track}} = \sqrt{P_x^2 + P_y^2} \tag{5.2}$$

- P_T^{miss}
  The missing transverse momentum of the event. It is a good measure for the neutrino identification. But not only neutrinos contribute to the P_T^{miss}, but also particles escaping the detection (by cracks, dead material, outside the detector acceptance). P_T^{miss} is defined as sum of the transverse momentum of all combined objects in the event

$$\left(P_T^{\text{miss}}\right)^2 = \Big(\sum_{\text{Combined Objects}} P_x \Big)^2 + \Big(\sum_{\text{Combined Objects}} P_y \Big)^2 \tag{5.3}$$

- P_T^{X}
  The transverse momentum of the hadron vector X, which is defined as the HADFS excluding the contributions from the identified lepton jet. The hadron vector corresponds to the b-jet. In analogy to P_T^{miss} it loops only over the combined objects, that are not part of the one-prong jet.

- ΔR_{Track} and $\Delta R_{\text{Cluster}}$
  The distance measured in $\eta\phi$-space between the jet axis and the closest track (cluster) in the event outside the jet. This variable gives a measure of the isolation for the jet. It is defined as

$$\Delta R_{\text{Track}} = \min \left(\sqrt{\left(\eta_{\text{op track}} - \eta_{\text{event track}}\right)^2 + \left(\phi_{\text{op track}} - \phi_{\text{event track}}\right)^2} \right) \tag{5.4}$$

  where *op track* refers to the one-prong track in the jet and *event track* to all other tracks found in the event. $\Delta R_{\text{Cluster}}$ is defined in analogy.

- $E_{\text{Jet}}/p_{\text{Track}}$
  The ratio of the jet energy and the momentum of the track in the jet.

- $E_{\text{F-level}}/E_{\text{1-level}}$
  The reconstruction software of the LAr calorimeter performs corrections to the measured electromagnetic energy. There are 3 major levels of measuring the energy: The 0-level, which is the raw measured electromagnetic energy in the Calorimeter. The 1-level, which has the dead material correction added and the F-level, which applies a correction factor to all hadronic particles for compensation (see also chapter 3.2.2). Since electrons are expected to be stopped within the ECAL, the application of this correction is based on an energy deposit in the HCAL. The variable $E_{\text{F-level}}/E_{\text{1-level}}$ is defined as ratio calculated as the energy of the F-level over the energy of the 1-level.

- $\Delta\Phi_{\text{l-X}}$
  Azimuthal difference between the lepton jet and the hadron vector X, defined as

$$\Delta\Phi_{\text{l-X}} = \phi_{\text{thrust}} - \phi_{\text{X}} \tag{5.5}$$

- V_{ap}/V_p
  A measure of the azimuthal balance of the event. It gives a measure of the balance of the calorimetric energy deposits in the LAr.

$$\begin{aligned}
(E_x, E_y) &= E_{\text{Cluster}} \cdot (P_{T,x}, P_{T,y}) \cdot \frac{1}{P_T} && (5.6)\\
(V_x, V_y) &= \sum_{\text{Cluster}} (E_x, E_y) && (5.7)\\
V &= \sqrt{V_x^2 + V_y^2} && (5.8)\\
P_{T,proj}^{\text{Track}} &= \frac{1}{V}\begin{pmatrix} V_x \\ V_y \end{pmatrix} \cdot \begin{pmatrix} E_x \\ E_y \end{pmatrix} && (5.9)
\end{aligned}$$

$$\begin{aligned}
V_p &= \sum_{\text{Clusters}} |P_{T,proj}^{\text{Track}}| \qquad \text{for} \quad P_{T,proj}^{\text{Track}} > 0 && (5.10)\\
V_{ap} &= \sum_{\text{Clusters}} |P_{T,proj}^{\text{Track}}| \qquad \text{for} \quad P_{T,proj}^{\text{Track}} < 0 && (5.11)
\end{aligned}$$

  The variable was originally defined for a CC analysis [34].

- Charge
  The electromagnetic charge of the isolated particle. It is determined from the curvature of the track in the tracking chamber due to the magnetic field. This determination is limited by the resolution of the curvature and the transverse momentum

$$\frac{\Delta P_T^{\text{Track}}}{P_T^{\text{Track}}} = 2\% \cdot P_T^{\text{Track}}. \tag{5.12}$$

  The charge will be determined for transverse momenta up to ~ 50 GeV.

5.5 The Preselection

As seen in chapter 2, the topology of an Anomalous Top Production event is quite restrictive:

- At least two jets in the event with rather high energies
- High missing transverse momentum due to two neutrinos

These criteria were used to make a preselection. For further reduction of background events only the central region is considered. The preselection demanded at least 2 jets, whereas one jet included at least one track with P_T^{track} larger than 3 GeV and within the central region ($|\eta| < 1.7 \quad (20^\circ - 159^\circ)$).

The preselection requirements are summarized in table (5.2).

Cut values for the Preselection	
Variable	Value
# Jets	2+
P_T^{miss}	> 12 GeV
At least one jet with Track requirements:	
P_T^{track}	> 3 GeV
$\|\eta\|$	$< 1.7 \quad (20^\circ - 159^\circ)$

Table 5.2: Preselection Cuts used to reduce the large data sample.

The distribution for P_T^{track} is given in Fig. (5.3) for the Monte Carlo simulation. The cut at 3 GeV is performed to reduce background. The peak of the distribution is between 5 GeV and 10 GeV.

This preselection process selected 9428 events of the 2000 data and 2472 events of the 1999 data, corresponding to a reduction factor of roughly 10^4. In a next step, these remaining 11'900 events were searched for a more specific topology: The one-prong requirement for at least one jet was added and the angular acceptance was narrowed to $|\eta| < 1.5 \quad (25^\circ - 154^\circ)$. This reduced the sample to 2911 events, which served as basis for the final analysis and are referred to as *final sample*.

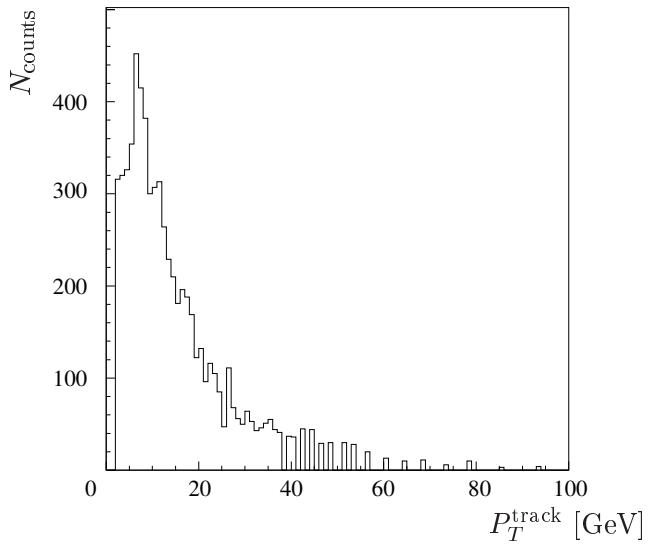

Figure 5.3: The P_T^{track} distribution for Monte Carlo reconstructed top decay. The P_T^{track} refers to the transverse momentum of a track inside a one-prong jet with $|\eta| < 1.5$. At least two jets were required, the P_T^{miss} requirement was set on 12 GeV. The lower edge is cut at 2 GeV, the peak is located around 8 GeV.

5.6 Final Analysis

The final sample was studied in detail, using the sensitive variables defined in chapter 5.4. From the MC simulation 24% of the events passed the preselection process. The large reduction of 76 % mainly arises from the hard P_T^{track} cut and the geometrical restriction in the preselection. These events determine the *signal region* whereas the 2911 events from the data determine the *background region*. This view was justified as at most a few events in the data are expected originating from the Anomalous Top Production.

To optimize the signal-to-background ratio the following kinematical cuts were developed (summary in table (5.3)). The figures generally show the distributions after the preselection cuts defined in table (5.2) for the simulated events from the MC as open histogram and the ones of the data[1] as hatched histogram.

- $P_T^{\text{miss}} > 25$ GeV

  The decay chain of the top into the hadronic one-prong decay (Fig. (5.1)), includes two neutrinos and hence a large P_T^{miss}. Fig. (5.4) shows the simulated event distribution for P_T^{miss} with the peak at large values as expected. After the preselection process, the P_T^{miss} requirement was tightened to 25 GeV in agreement with the isolated lepton search. The reduction of background with a cut of $P_T^{\text{miss}} > 25$ GeV is 81 %.

[1] combined data from 1999 and 2000

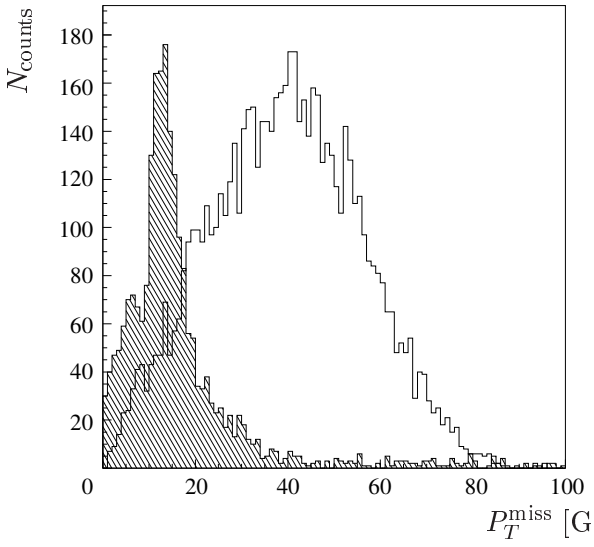

Figure 5.4: The P_T^{miss} distribution for Monte Carlo reconstructed top decay (open histogram) and the data (hatched histogram) after the preselection cuts as defined in table (5.2).

- $P_T^{\text{X}} > 25$ GeV

The hadron vector X comes from a high energetic b-jet, a rather hard cut at 25 GeV is reasonable as clearly visible in Fig. (5.5).

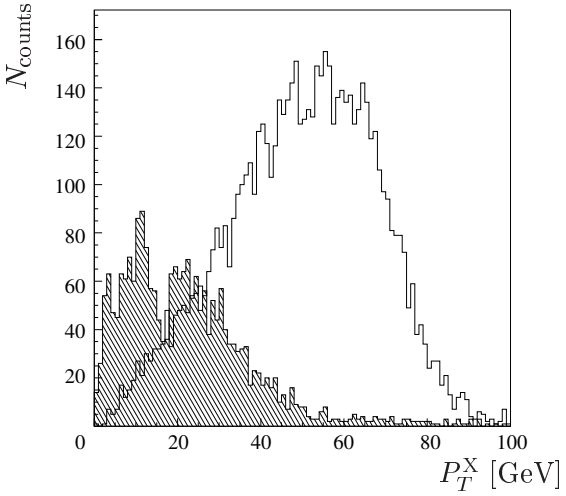

Figure 5.5: The P_T^{X} distribution for Monte Carlo reconstructed top decay (open histogram) and the data (hatched histogram) after the preselection cuts.

- $\Delta R_{\text{Track}} < 3$ and $\Delta R_{\text{Cluster}} < 2$

The theoretical considerations would lead to a minimum value for ΔR_{Track} ($\Delta R_{\text{Cluster}}$) since the one-prong jet is isolated. Looking at Fig. (5.6), the isolation in the signal (open histogram) is visible, but the data (hatched histogram) show an even more isolated topology. The explanation is rather simple. The preselection process already selects events with separated jets, and the main part of it is in a back-to-back topology, represented by $\Delta R_{\text{Track}} = \Delta R_{\text{Cluster}} = \pi$. This back-to-back topology

comes from two-body decays of particles at rest. The result is an upper value for the isolation of the one-prong jet.

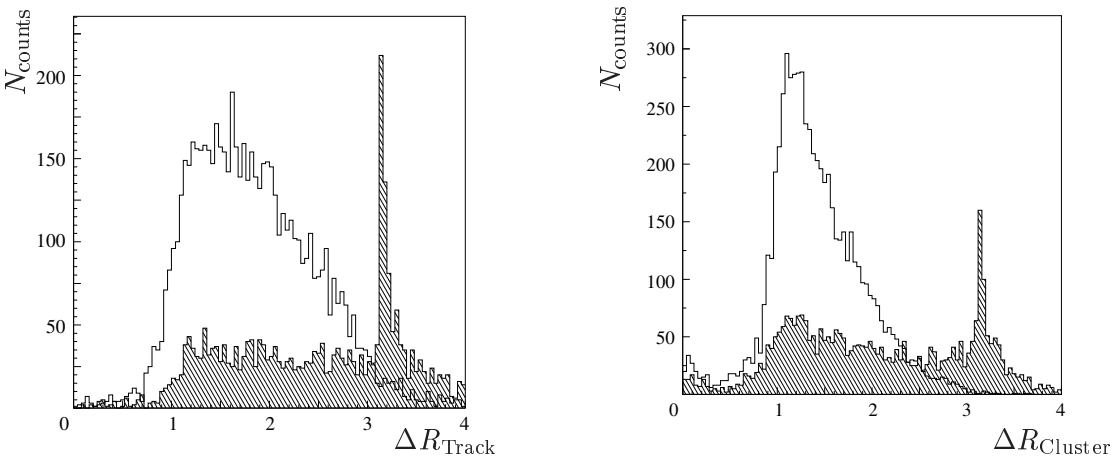

(a) The ΔR_{Track} distribution

(b) The $\Delta R_{\text{Cluster}}$ distribution

Figure 5.6: Monte Carlo (open) and data (hatched) for the isolation criteria after the preselection cuts.

Note that, Fig. (5.6(a)) shows entries below 1, even though the jet radius was set to be 1 and therefore no other track within the jet is allowed. These entries occur due the fact that the one-prong track is not necessarily in the center of the jet.
The entries in Fig. (5.6(b)) close to zero, maybe due to γ's from the decay $\pi^0 \to \gamma\gamma$. Even though the π^0 is expected close to the charged pion, there are decays with up to 4 π^0's possible.

- $E_{\text{Jet}}/p_{\text{Track}} > 0.8$

The energy of the jet is expected to be greater than the energy of the charged pion, since the π^0's contribute to the jet energy but not to the track momentum. Therefore an $E_{\text{Jet}}/p_{\text{Track}}$ value of clearly above 1 is expected to be characteristic for a top decay. Fig. (5.7) shows the $E_{\text{Jet}}/p_{\text{Track}}$ distributions for the Monte Carlo events (open histogram) and the data (hatched histogram).

The peak for the signal is clearly visible at 1. The explanation is rather simple: The H1-Detector has several internal algorithms for energy correction mentioned in chapter 3.2.2. One of them is tuned to set the ratio of Energy/momentum of particles as close to the value of 1 as possible. The motivation is the assumption of a particle being stopped in the detector, and therefore all energy is to be deposited in the calorimeter. The momentum of the particle is used as reference for the calibration

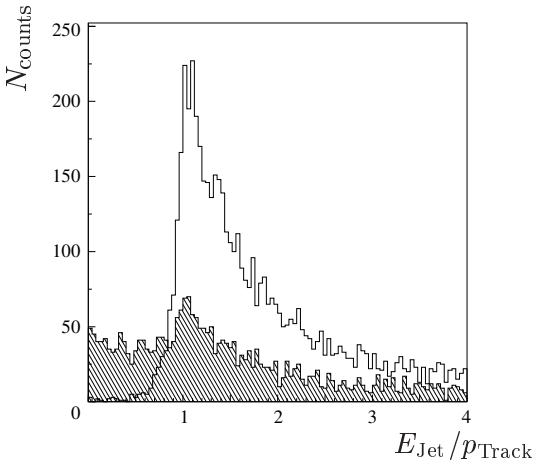

(a) The $E_{\text{Jet}}/p_{\text{Track}}$ distribution for the data (hatched) and the simulation of Anomalous Top Production (open).

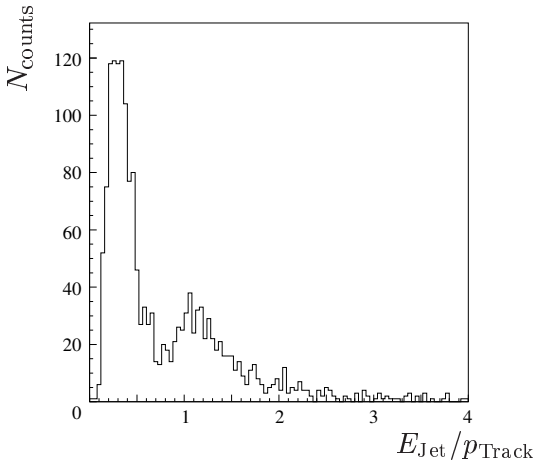

(b) $E_{\text{Jet}}/p_{\text{Track}}$ for EPVEC muons. Rejection for $E_{\text{Jet}}/p_{\text{Track}}$ ¡ 0.8.

Figure 5.7: The $E_{\text{Jet}}/p_{\text{Track}}$ distributions after the preselection cuts.

of the calorimeter.

This makes it nearly impossible to distinguish between a single charged particle, and a charged particle accompanied with several neutral particles, entering the calorimeter very close together. The energy deposits can not be assigned to the different particles (the detector can only measure the momentum of charged particle tracks) and are treated as one single energy deposit. In the case of the high energetic τ jet the energy of the decay products are all added together, as desired. The calorimeter now uses the calibration reference from the charged pion track and returns a rescaled energy.

One possible solution is to compare the energies before and after the calibration. This has been done and is described by the variable $E_{\text{F-level}}/E_{\text{1-level}}$ described in Fig. (5.8).

Nevertheless the $E_{\text{Jet}}/p_{\text{Track}}$ variable was useful: It was used to reduce the muons in the data. Since the muons pass through the entire detector their momentum is greater than the deposited electromagnetic energy in ECAL and HCAL. Fig. (5.7(b)) shows this characteristic for the μ simulated by the EPVEC Generator as peak between 0.2 and 0.4.

- $E_{\text{F-level}}/E_{\text{1-level}} > 1.1$

  For electrons the ratio of F-level energy to 1-level energy is expected to be 1 and for pions (hadrons) it corresponds to the correction factor of roughly 1.3. Fig. (5.8(a)) shows the distribution of the the ratio $E_{\text{F-level}}/E_{\text{1-level}}$ versus the Particle Code (PC[2]) for MC simulated events. One sees clearly the difference between hadrons (π^+ PC= 211) and leptons (e^+ PC= -11).

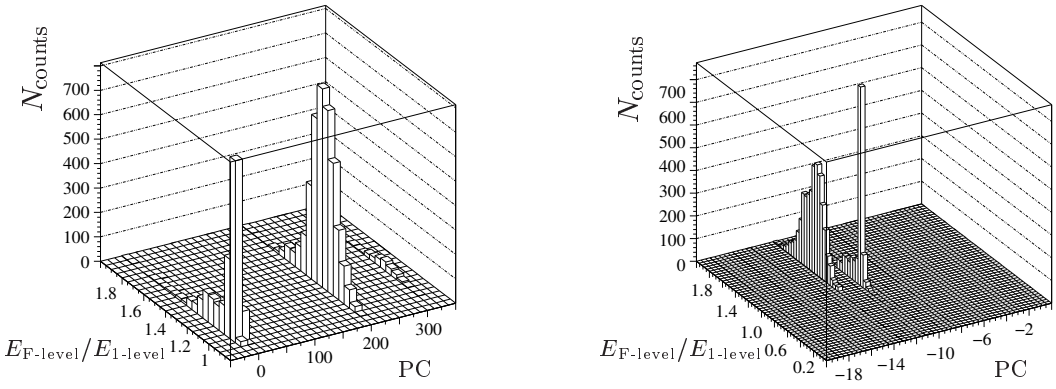

(a) τ decay from the Anomalous Top Production where the τ decays in one charged pion.

(b) muonic decay of W

Figure 5.8: The $E_{\text{F-level}}/E_{\text{1-level}}$ versus particle code distribution after the preselection cuts.

  There is also a very small peak at particle code 321, corresponding to the Kaons (K^+). This distribution also demonstrates the dominance of the pions over the kaons. Muons, as the only leptons to pass through the HCAL, will get this correction to their energy deposit as well (see Fig. (5.8(b))). The $E_{\text{F-level}}/E_{\text{1-level}}$ variable enables to distinguish between the electron background and the pion signal.

- $\Delta\Phi_{\text{l-X}} < 2.8$

  The data passing the preselection show a clear back-to-back topology where $\Delta\Phi_{\text{l-X}}$ peaks at the value of π (See Fig. (5.9) hatched histogram). The Monte Carlo simulation shows a peak at $\sim$2.6. This is due to the two neutrino decays: The b-jet is back-to-back to the W, but the τ as well as the π^+ get a deviation in their flight direction relatively to the flight direction of the mother particle, due to the neutrinos and momentum conservation.

[2]The PC corresponds to the Monte Carlo numbering scheme introduced in 1988 by the Particle Data Group [35]

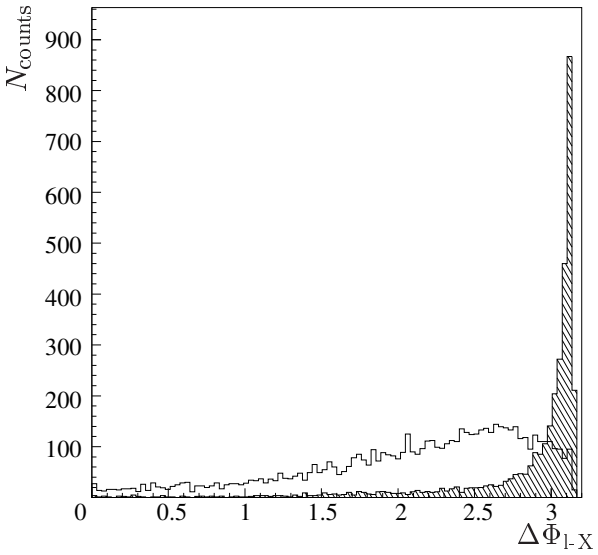

Figure 5.9: The $\Delta\Phi_{\text{l-X}}$ distribution for the data from H1 (hatched) and the Monte Carlo for Anomalous Top Production (open) after the preselection cuts. The hatched histogram shows a strong back-to-back topology.

- V_{ap}/V_p

The top decay splits the space in two hemisphere, one is occupied by the b-jet the other with the W. The b-jet deposits quite a lot energy, but the energy deposit from the W, in the case of a τ decay, looses energy in two neutrinos. This results in a low expected value for V_{ap}/V_p for Anomalous Top Production. The background is expected to have a rather balanced energy deposit. In fig (5.10) the low V_{ap}/V_p values for the MC simulated top is clearly visible. The open histogram has 58 % of the entries at values less than 0.2, whereas the data (hatched) has only 13.5 % of the entries in the same region.

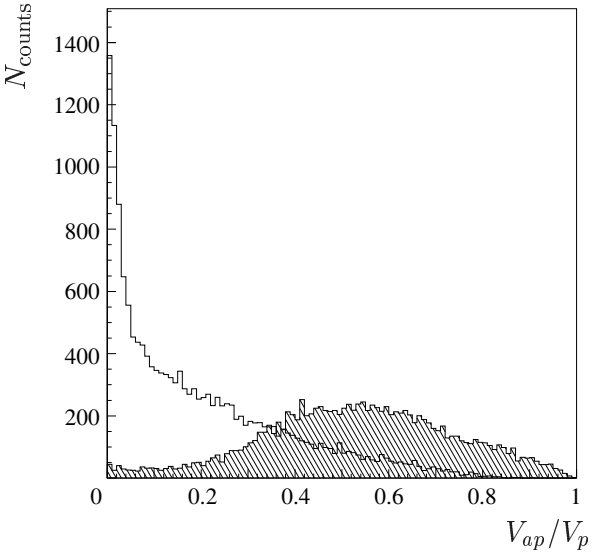

Figure 5.10: The V_{ap}/V_p distribution for data (hatched) and simulated events (open) after the preselection cuts.

But despite the obvious difference between signal and background, V_{ap}/V_p was not used as requirement. This is due to a correlation of V_{ap}/V_p with $\Delta\Phi_{\text{l-X}}$, visible in Fig. (5.11) for Monte Carlo and the data.

After the previous kinematical cuts, no event had a V_{ap}/V_p value above 0.2, so an additional cut on that variable would not yield in a further reduction.

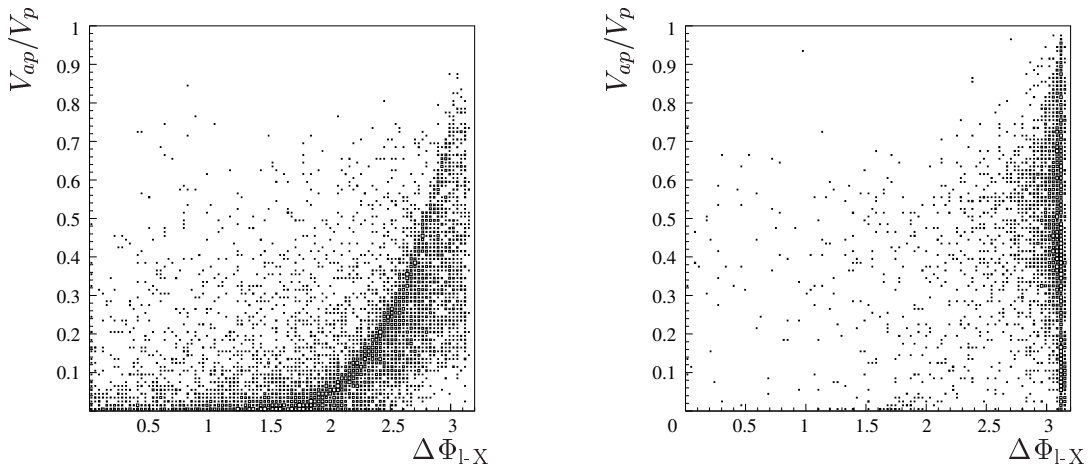

(a) Monte Carlo simulation

(b) data

Figure 5.11: V_{ap}/V_p versus $\Delta\Phi_{\text{l-X}}$ after the preselection cuts. The correlation is well to detect: The MC simulation shows a directly proportionality. The data on the other side has almost no entries at low $\Delta\Phi_{\text{l-X}}$, and even less at low $\Delta\Phi_{\text{l-X}}$ and low V_{ap}/V_p. Therefore the kinematical requirement for $\Delta\Phi_{\text{l-X}}$ is sufficient for both variables.

- Charge > 0

The coupling of the top to the light quarks is dominated by the $\kappa_{\gamma,u}$ contribution. The flavour change of the u to the top, yields a positively charged top, and the decay chain will contain only positively charged particles. A cut on the charge of the isolated particle is justified. In the Monte Carlo simulation, only 0.3 % of the isolated particles passing the kinematical requirements from above have a negative charge.

All cut variables and their values are summarized in table (5.3).

Cut Values for Final Analysis			
Variable	Value	Variable	Value
Subtrigger	67 or 77	$E_{\text{Jet}}/p_{\text{Track}}$	> 0.8
P_T^{miss}	> 25 GeV	$E_{\text{F-level}}/E_{\text{1-level}}$	> 1.1
P_T^{X}	> 25 GeV	$\Delta\Phi_{\text{l-X}}$	< 2.8
ΔR_{Track}	< 3	Charge	> 0
$\Delta R_{\text{Cluster}}$	< 2		

Table 5.3: Kinematical cut values used for the final analysis

5.7 Calculating the Efficiency

The *Efficiency* ε expresses the ratio of selected events over all events. It is only defined for the selection process applied on Monte Carlo simulation. In case of the signal the efficiency is defined as

$$\varepsilon_{\text{Signal}} = \frac{N_{\text{found and reconstructed events}}}{N_{\text{generated events}}} \tag{5.13}$$

Table (5.4) gives the number of selected candidates after the corresponding cut was applied. Please note, that it is highly dependent on the ordering of the applied cuts.

Efficiencies for the Sensitive Variables		
Sensitive variable	signal	data
Starting Sample	25'000	10^8
After Preselection (events)	5'991	2'911
After Preselection (candidates)	6'418	3'278
P_T^{miss}	5'318	407
Subtrigger	5'315	356
$E_{\text{Jet}}/p_{\text{Track}}$	4'966	182
$E_{\text{F-level}}/E_{\text{1-level}}$	3'614	99
P_T^{X}	3'460	50
ΔR_{Track}	3'377	8
$\Delta R_{\text{Cluster}}$	3'160	7
$\Delta\Phi_{\text{l-X}}$	2'800	3
Charge	2'771	0
Final Result	**2'771**	**0**
Total Efficiency	11.1 %	—

Table 5.4: The efficiency for the signal and the reduction of the data, where the number corresponds to the number of selected events after the specified cut was applied.

There was no requirement demanding only one one-prong jet per event. So it is possible to have more than one candidate in an event after the preselection. Two candidates in an event may arise from scattered electrons or other single particles penetrating the detector.

5.8 Result

The detailed analysis of the decay chain

$$t \to Wb, W \to \tau\nu_\tau, \tau \to \pi\,(n\pi^0)\,\nu_\tau \tag{5.14}$$

of the complete H1 data sample from the years 1999 - 2000 with an integrated luminosity of 62.76 pb^{-1}found no events. The resulting upper limits for the production cross section are being calculated in the next chapter.

Chapter 6

The Cross Section for Anomalous Top Production

The goal of the analysis was the search for Anomalous Top Production. The result will be presented as cross section for Anomalous Top Production $\sigma(ep \to e'tX)$ at H1, or as an upper limit depending on the interpretation of the found event. There are several possibilities for reporting the results. Small samples are handled by the poisson statistics and yield an upper limit for the production cross section.

6.1 Production Cross Section

The production cross section is defined as

$$\sigma(ep \to e'tX) \equiv \frac{N}{\mathcal{L}B\varepsilon} \tag{6.1}$$

N is the number of found events, B is the total branching ratio for the specified decay channel and ε is the total efficency for an event to be detected in the detector.

The Branching Ratios[19] of all considered decays are summarized in table (6.1).

The decay of the top is assumed to be SM like. In the Monte Carlo simulation, the decay of the τ is only generated for the hadronic decays, which have a BR of 64.8 %. The MC efficency is calculated in table (5.4) and the trigger efficency is provided by [24]. The integrated luminosity is 62.76 pb^{-1}.

The formula for the production cross section becomes

$$\sigma(ep \to e'tX) = \frac{N}{\mathcal{L} \cdot \big(B(t \to Wb)\, B(W \to \tau\nu_\tau)\, B(\tau \to \text{hadrons})\big) \cdot \varepsilon_{\text{tot}}} \tag{6.2}$$

The error is calculated on the equation (6.2) and attached to table (6.1).

All considered Branching Ratios, Efficiencies and the Errors		
Variable	Value	Error
Luminosity $\mathcal{L}$	62.76	$\pm$ 0.94 (1.5 %)
$B(t \to Wb)$	100 %	no error
$B(W \to \tau\nu_\tau)$	10.4 %	$\pm$ 0.4 %
$B(\tau \to$ hadrons)	64.8 %	$\pm$ 0.09 %
Trigger Efficency	99%	$^{+1}_{-0}$%
Total error		$\pm$ 1.85 %

Table 6.1: List of all considered branching ratios and efficiencies including the errors.

Since no event was found, a production cross section can not be calculated.

6.2 Upper Limit

In case of an upper limit instead a production cross section, the number of found events is considered as poisson distribution. The confidence limits are expressed by N_{limit}, where N_{limit} is the 90 % confidence interval (lower/upper bound $\mu_{1/2}$) for n_0 observed events in absence of background [19] and are displayed in Fig. (6.1).

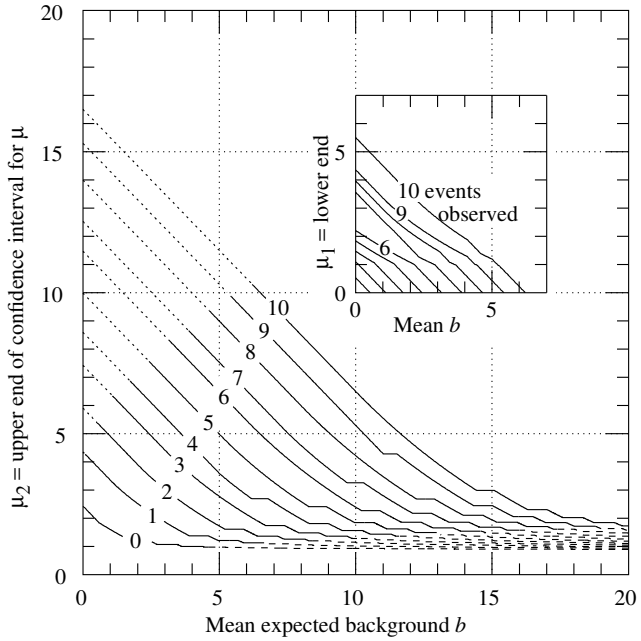

Figure 6.1: Poisson statistic for small samples. 90 % confidence intervals $[\mu_1, \mu_2]$ on the number of signal events as a function of the expected number of background [19].

The formula for an upper limit has become

$$\sigma(ep \to e'tX) = \frac{N_{\text{limit}}(n_0)}{\mathcal{L} \cdot \big(B(t \to Wb)\, B(W \to \tau\nu_\tau)\, B(\tau \to \text{hadrons})\big) \cdot \varepsilon_{\text{tot}}} \tag{6.3}$$

6.2.1 Background Estimation

The number of observed events n_0 in presence of background is defined as

$$n_0 = N_\tau + N_\mu + N_{\text{SM}} \tag{6.4}$$

where the N_τ and N_μ refer to the number of events found in the corresponding leptonic channel of the W decay. N_{SM} is the sum of all events found in the considered SM-background contributions discussed in chapter 4.2.

To estimate the expected background contributions from the SM, separate simulations were studied and analyzed identically. The number of events found in these background simulations are summarized in table (6.2).

SM Background and Muonic W Decay				
Background	MC Generator	Events found	$\mathcal{L}$	expected
SM W-production $W \to \mu\nu_\mu$	EPVEC	75	10^5pb^{-1}	0.05
SM W-production $W \to \tau\nu_\tau$	EPVEC	303	10^5pb^{-1}	0.19
Lepton Pair-production	LPAIR	0	10^3pb^{-1}	0
SM Jets	PYTHIA	0	16pb^{-1}	0
muonic top decay	SUSYGEN	538	—	0.19

Table 6.2: All background contributions with the expected events in the visible kinematical region. The low integrated luminosity for the PYTHIA generator yields a large statistical error.

The number of found events has to be normalized to the integrated luminosity of the data by the equation

$$N_{\text{normalized}} = N_{\text{actual}} \cdot \frac{\mathcal{L}_{\text{Data}}}{\mathcal{L}_{\text{MC Simulation}}} \tag{6.5}$$

In case of the muonic decay of the top

$$t \to Wb\,, \quad W \to \mu\nu_\mu \tag{6.6}$$

the relative normalization is identically since both Monte Carlo files contain 25'000 simulated events. This yields a ratio of

$$\frac{N_\tau}{N_\mu} = \frac{5}{1}. \tag{6.7}$$

The low number of selected muon events is due to the optimization of the selection process for the τ decay. The kinematical cut on $E_{\mathrm{Jet}}/p_{\mathrm{Track}}$ reduces the muons by one order of magnitude.

The contribution of the SM W production is calculated to be 0.05 and 0.19 events for the muon and the tau channel, respectively. The lepton pair production and SM jet production are expected to be zero. The total expected background from the SM adds up to 0.24 events. Please note that the statistical error is quite large due to the low integrated luminosity for the PYTHIA generator.

The error for an upper limit can be conservatively added to N_{limit} according to

$$\sigma(ep \to e'tX) \leq \frac{N_{\mathrm{limit}}}{k \pm \delta k} \leq \frac{N_{\mathrm{limit}} \cdot (1 + \frac{\delta k}{k})}{k} \tag{6.8}$$

N_{limit} is determined for the 90 % CL using Fig. (6.1) and the 95 % CL the corresponding table in [19].

For $n_0 = 0$ we get $N_{\mathrm{limit}} = 2.44$ (3.09) for 90 % (95 % CL), and as upper limit for the production cross section

$$\sigma(ep \to e'tX) \leq 5.4 \quad pb \qquad \text{at 90 \% CL} \tag{6.9}$$

$$\sigma(ep \to e'tX) \leq 6.8 \quad pb \qquad \text{at 95 \% CL} \tag{6.10}$$

Chapter 7

Conclusion and Outlook

The search for anomalous top decaying via W in the third leptonic generation has been done for the first time at HERA. The decay into a τ and the leptonic decay thereof involves two neutrinos, which makes a full reconstruction impossible.

Within the data taken at H1 in the years 1999 - 2000, the selection process found

0 event, 0.24 expected.

The upper limit for the production cross section was calculated to be

$$\sigma(ep \to e'tX, \sqrt{s} = 320 \text{ GeV}) \leq 6.8pb \qquad \text{at } 95 \text{ \% CL} \tag{7.1}$$

The previous search in the first two lepton generations achieved an upper limit for the production cross section [15] of

$$\sigma(ep \to e'tX, \sqrt{s} = 320 \text{ GeV}) \leq 0.87\, pb \qquad \text{at } 95 \text{ \% CL} \tag{7.2}$$

The upper limit derived from the present analysis is compatible with this value.

As a conclusion from this analysis, no anomalous top was found in the considered decay chain and therefore the FCNC via the coupling $\gamma - u - t$ (Fig. (2.4(a))) is not expected as dominating process for BSM.

The kinematical requirements also qualify for a search for *lepto-quarks*. The only modification would be to remove the last kinematical cut ($\Delta\Phi_{\text{l-X}}$) since the lepto-quark decay is expected in back-to-back topology as well as the charge requirement . Table (5.4) shows 7 events selected by the present analysis before the $\Delta\Phi_{\text{l-X}}$ requirement but none of these events classifies as lepto-quark candidate.

A further analysis has to confirm the presented results. Improvements on the selection process can be done by considering

- increasing the efficency by optimization of the kinematical cuts,
- using the cell level information for the calorimeter energies rather than the cluster level,
- looking for more specific signatures in the energy calibration,
- developing a π^0 identification algorithm,
- the fact, that the charged pion track will not point to the primary vertex,
- including more τ decay channels, such as kaons, three prong decays, leptonic decays,
- a more detailed study of the background.

Chapter 8

Acknowledgments

After 5 years studying physics at the ETH Zurich, my studies finally come to an end. This closing work was enabled by Prof. Dr. R. A. Eichler, whom I want to thank very much for giving me the opportunity and the motivation to be a part of the H1 Collaboration. Also special thanks goes to Dr. C. Grab, who supported and guided me through the entire analysis. J. Gassner and M. Hilgers are also mentioned. I want to thank them for their patience and continuing support concerning the technical and physical problems encountered during the analysis. I am very grateful to R. Bächli, who did a great job with the administration.
I also owe great thanks to A. Schoening at Hamburg, who inspired me and gave many helpful hints. I very much enjoyed the discussions I had with him.

Appendix A

Event Display

The following pages show four events, selected by the selection algorithm defined in chapter 5 at different stages. The visual scan identified two as cosmics, both were rejected by the electromagnetic charge requirement only. The events will be shown in the H1 event display as explained in Fig. 4.1.

The table below summarizes the kinematics of the four events.

Event Kinematics				
Kinematical variable	137400	245481	119854	34493
Subtrigger	ST67 and ST77	ST67 and ST77	ST67 and ST77	ST67 and ST77
P_T^{miss} [GeV]	36.4 (33.2)	29.6 (23.8)	93.7 (89.2)	69.7 (69.2)
P_T^{X} [GeV]	32.1	129.8	90.4	69.0
V_{ap}/V_p	0.19	0.82	0.02	0.001
P_T^{track} [GeV]	3.56	44.5	3.15	5.45
$E_{\text{Jet}}/p_{\text{Track}}$	1.65	2.35	2.33	1.51
$E_{\text{F-level}}/E_{\text{1-level}}$	1.42	1.12	1.55	1.29
ΔR_{Track}	0.78	2.69	1.38	1.35
$\Delta R_{\text{Cluster}}$	1.11	1.70	1.62	1.03
$\Delta\Phi_{\text{l-X}}$	1.09	3.13	2.05	1.60
θ_{lepton} [°]	39.3	27.2	122.8	102.4
Charge	-1	+1	-1	-1
Interpretation of event	γp (?)	NC	cosmic	cosmic

Table A.1: The kinematics of four selected events

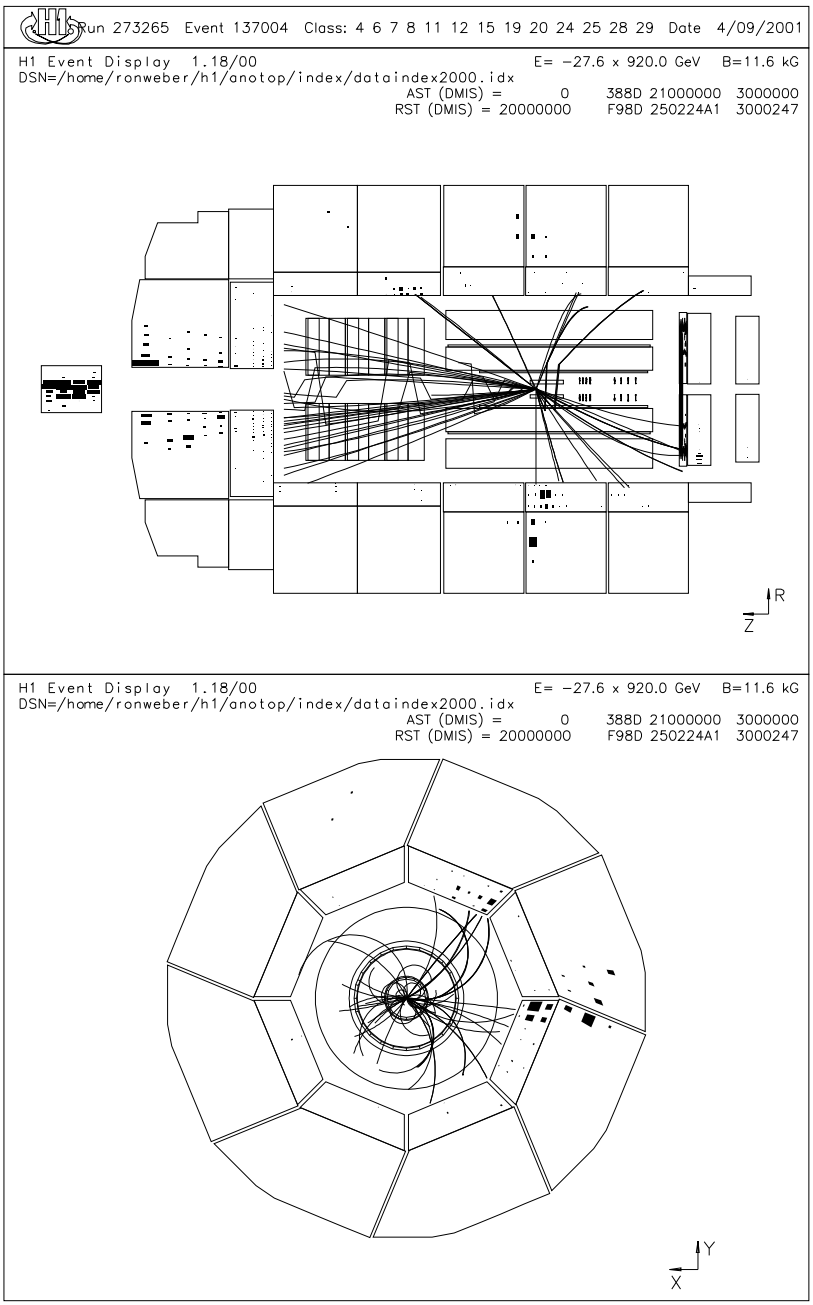

Figure A.1: This is a candidate event after the $\Delta\Phi_{\text{l-X}}$ cut in the event display (see Fig. 4.1). The isolated track (identified by the energy depositions) has 3.5 GeV and is well isolated in $\eta\phi$ (the tracks around the isolated one, are either low energetic or well separated only in η or ϕ).
The charge requirement removes this event from the candidate list. A possible origin of the event may be a γp interaction, with a high P_T proton remnant in the PLUG Calorimeter (square box on the far left) causing a high P_T^{miss}.

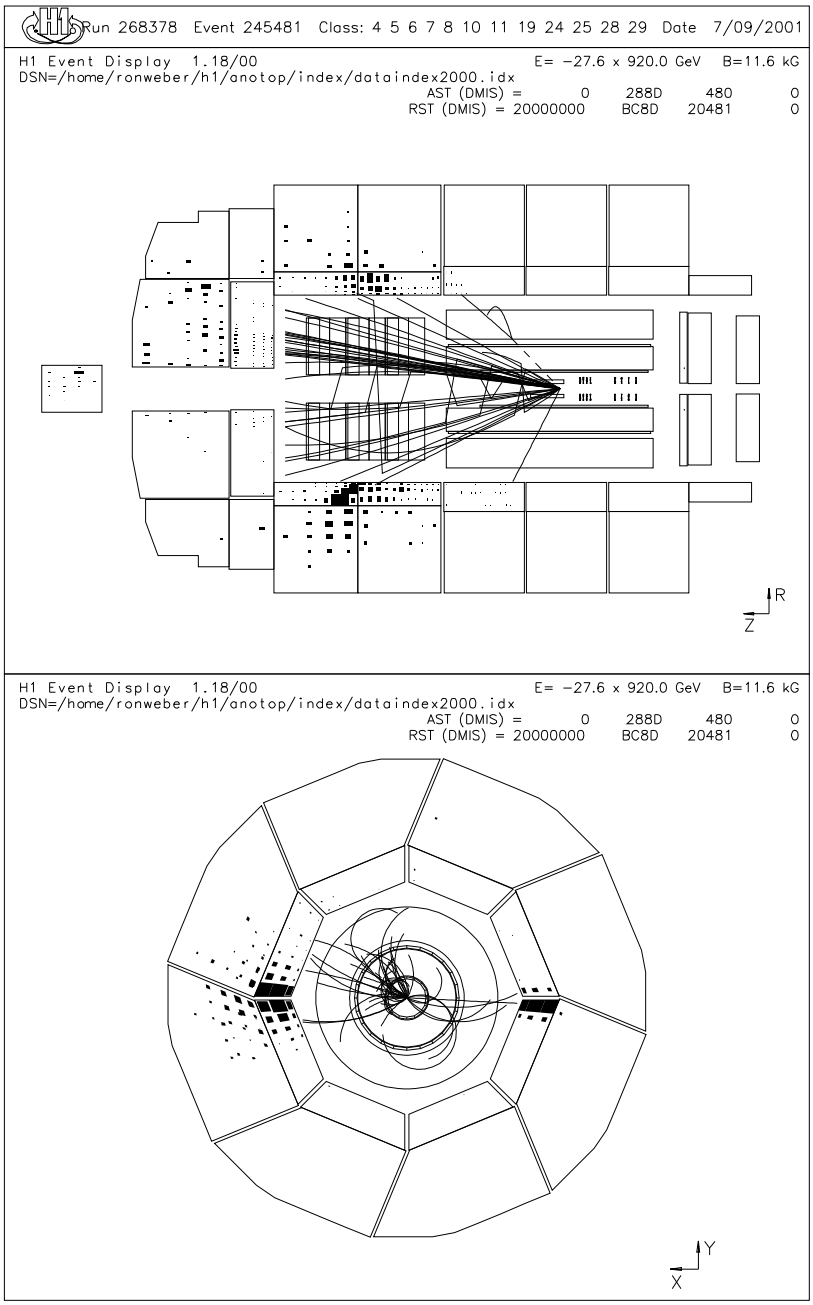

Figure A.2: This is a candidate event before the $\Delta\Phi_{\text{l-X}}$ cut in the event display. Therefore it would be within the candidates for lepto-quarks. The visual scan of the events identifies this event as NC interaction, with the electron and the jet pointing towards a crack where some energy is lost causing a high P_T^{miss}.

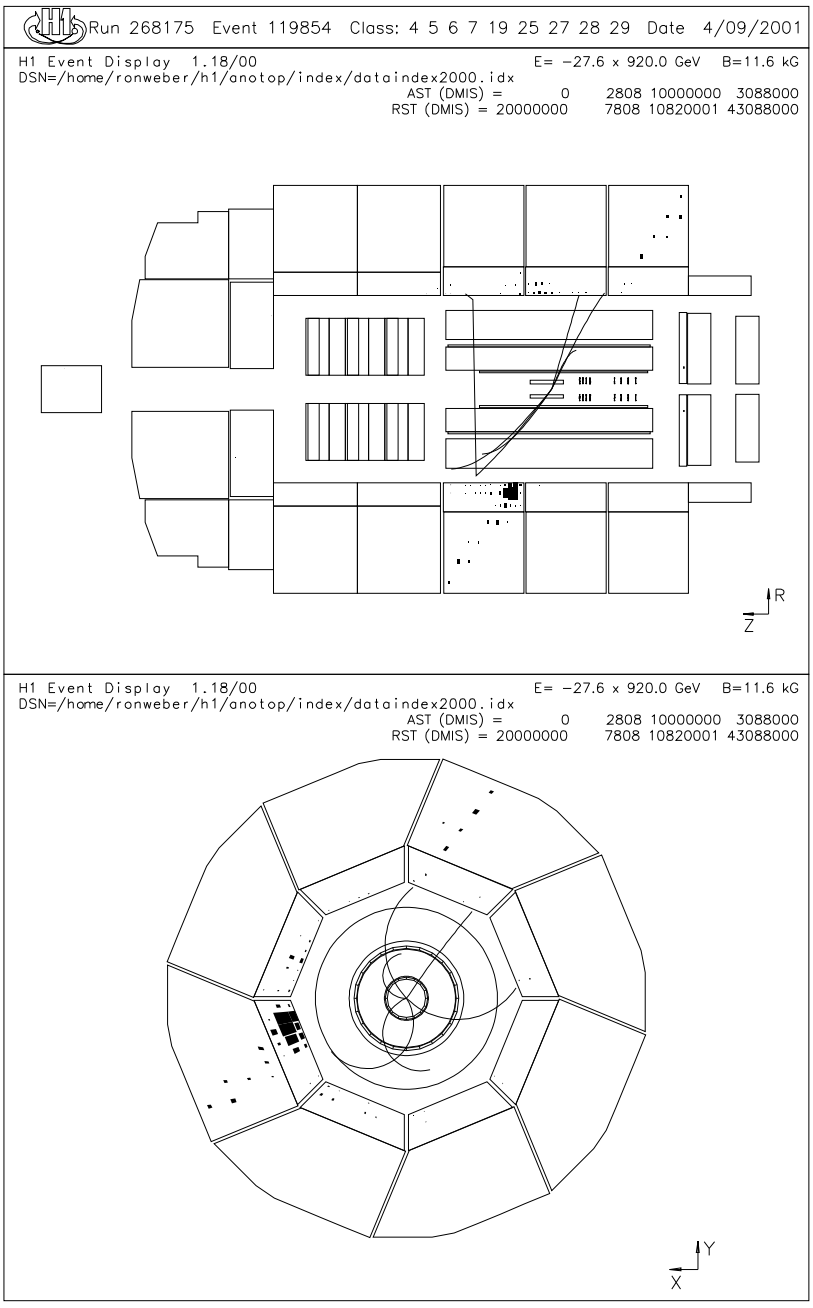

Figure A.3: This is a cosmic muon penetrating the detector. The muons enters from the top right corner (backward region) and shower in the detector leaving some low energetic particles and a large energy cluster on the opposite side. To get further information about the tracks and the cosmic muon, the additional tracking information stored on the *POT* is required.

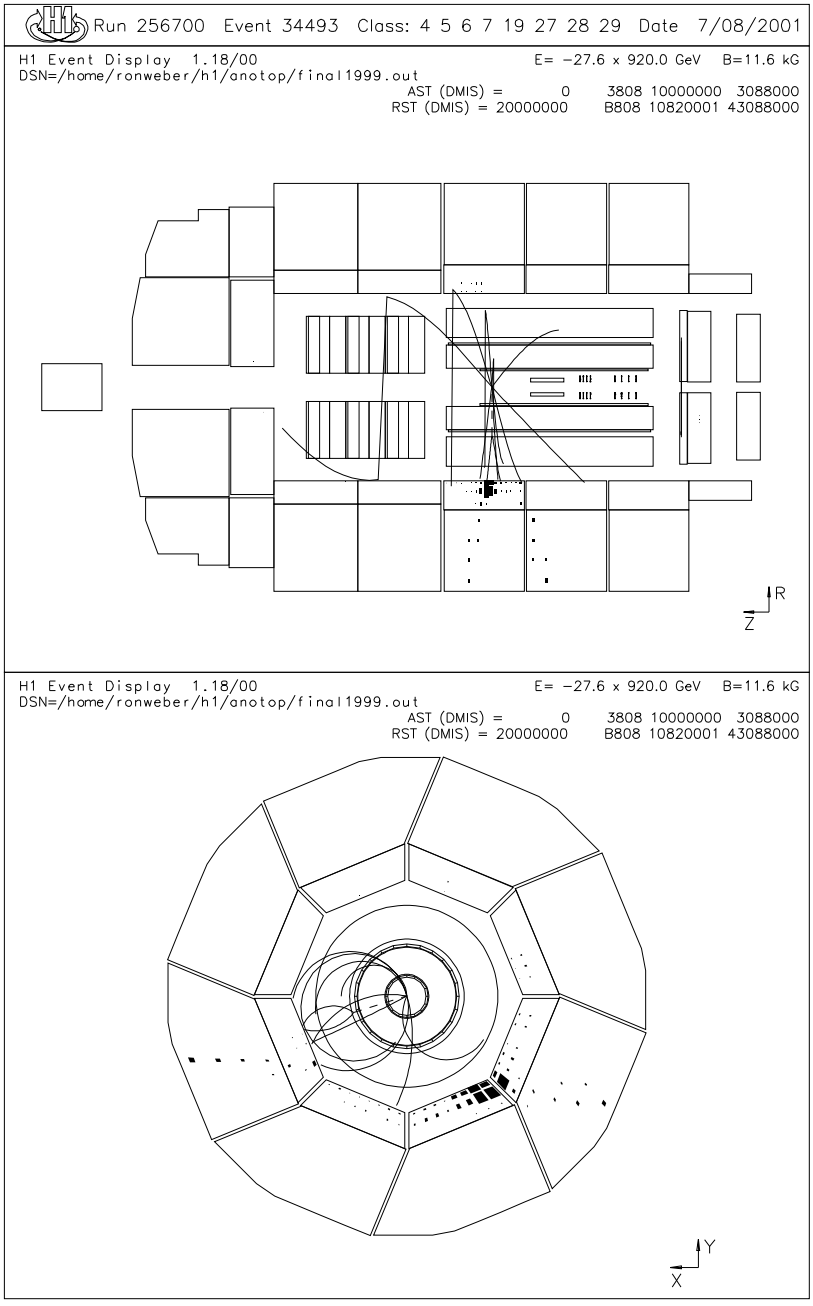

Figure A.4: A horizontal cosmic muon, entering from the left side (forward region) and showering. The high P_T track may result from remnants of beam-gas interactions reaching the detector at the same time. There is no obvious correlation between the high P_T track and the cosmic muon. To get further information about the origin of these tracks, the additional data from the POT is required.

List of Figures

2.1 ep scattering (general) . . . 6
2.2 Deep inelastic ep scattering . . . 7
2.3 Leading order Feynman graph for photoproduction processes . . . 8
2.4 The Feynman graph for Anomalous Top Production . . . 9
2.5 The anomalous top decay . . . 10
2.6 The τ decay . . . 10

3.1 The HERA collider . . . 13
3.2 The H1 detector . . . 15
3.3 The H1 tracking system . . . 17
3.4 The central tracking chambers . . . 17
3.5 The LAr calorimeter . . . 19
3.6 The Luminosity system . . . 22

4.1 A simulated Anomalous Top Production event . . . 24
4.2 γp reaction producing a SM W . . . 26
4.3 Lepton pair production in $\gamma\gamma$ interaction . . . 26
4.4 Leading order Feynman graph for photoproduction . . . 27

5.1 The decay chain . . . 30
5.2 The structure of the Jet . . . 33
5.3 The P_T^{track} distribution . . . 37
5.4 The P_T^{miss} distribution . . . 38
5.5 The P_T^{X} distribution . . . 38
5.6 Isolation criteria . . . 39
5.7 The $E_{\text{Jet}}/p_{\text{Track}}$ distribution . . . 40
5.8 The $E_{\text{F-level}}/E_{\text{1-level}}$ distribution . . . 41
5.9 The $\Delta\Phi_{\text{l-X}}$ distribution . . . 42
5.10 The V_{ap}/V_p distribution . . . 42
5.11 V_{ap}/V_p versus $\Delta\Phi_{\text{l-X}}$ . . . 43

6.1 Poisson statistics for 90 % confidence intervals . . . 48

A.1 Event # 137004 – γp . . . 56
A.2 Event # 245481 – NC . . . 57

A.3 Event # 119854 – Comics 58
A.4 Event # 34493 – Cosmics 59

Bibliography

[1] A.P. Heinson, A.S. Belyaev and E.E. Boos, *Single top quarks at the Fermilab Tevatron*, Phys. Rev. **D 56** (1997), 3114

[2] E. Boos, L. Dudko and T. Ohl, *Complete calculations of W b anti-b and W b anti-b + jet production at Tevatron and LHC: Probing anomalous W t b couplings in single top production*, Eur. Phys. J. **C 11** (1999), 473

[3] X. Wang, Y. Kuang, H. Zhou, H. Wang and L. Zhang, *Single top quark production in e gamma collisions and testing technicolor models*, Phys. Rev. **D 60** (1999), 014002

[4] T. Han, M. Hosch, K. Whisnant, B. Young and X. Zhang, *Single top quark production via FCNC couplings at hadron colliders*, Phys. Rev. **D 58** (1998), 073008

[5] P. Chiappetta, A. Deandrea, E. Nagy, S. Negroni, G. Polesello and J. M. Virey, *Single top production at the LHC as a probe of R parity violation*, Phys. Rev. **D 61** (2000), 115008

[6] S. Bar-Shalom, D. Atwood and A. Soni, *CP violation in single top quark production and decay via p anti-p → t anti-b + X → W+ b anti-b + X within the MSSM: A possible application for measuring arg(A(t)) at hadron colliders*, Phys. Rev. **D 57** (1998), 1495

[7] H1 Collaboration, C. Adloff *et al.*, Euro. Phys. J. **C5** 575 (1998); N. Malden these proc.

[8] R.P. Feynman *Very high-energy collisions of hadrons*, Phys. Rev. Lett. **23** (1969), 1415.

[9] J. D. Bjorken, *Asymptotic sum rules at infinite momentum*, Phys. Rev. **179** (1969), 1547

[10] M. Gell-Mann *A schematic model of baryons and mesons*, Phys. Lett. **8** (1964), 214.

[11] G. Zweig, CERN Preprint TH-401 (1964).

[12] F. Halzen and A. D. Martin, *Quarks and Leptons: An Introductory Course in Modern Particle Physics* John Wiley & Sons, (1984)

[13] C. Peterson, D. Schlatter, I. Schmitt and P. M. Zerwas, Rev. Lett. **D27** (1983), 105.

[14] Paul Scherrer Institut, *Proceedings of the Summer School on Hadronic Aspects of Collider Physics* PSI (1994), 23, M. P. Locher (editor)

[15] H1 Collaboration, HEP Conference Budapest 2001 (2001)

[16] S.J. Brodsky, P. Hoyer, C. Peterson, and N. Sakai, Phys. Lett. **B93** (1980), 451; S.J. Brodsky, C. Peterson, and N. Sakai, Phys. Lett. **D23** (1981), 2745

[17] CDF Collaboration, F. Abe *et al.*, Phys. Rev. Lett. **80** (1998), 2525.

[18] T. Han and J.L. Hewett, Phys. Rev. **D60** (1999), 074015.

[19] The European Physical Journey, Review of Particle Physics 2000 (Vol 15)

[20] H. Fritzsch and D. Holtmannspötter, Phys. Lett. **B457** (1999), 1199

[21] H1 Collaboration, I. Abt *et al.*, *Nucl. Instr. and Meth.* **A386** (1997), 310 and 348.

[22] H1 Calorimeter Group, B. Andrieu *et al.*, *Nucl. Instr. and Meth.* **A336** (1993), 499 and **A350** (1994), 357

[23] Chr. Veelken *Search for muonic W decays with the H1 detector at HERA* Diploma Thesis, University of Hamburg (2001)

[24] J. Rauschenebrger *Die Messung von Wirkungsquerschnitten des geladenen Stroms in der Positron-Proton-Streuung mit dem H1 Detektor*, PhD Thesis, University of Hamburg (2001)

[25] SUSYGEN 3.0/0.6 N. Ghodbane, S. Katsanevas, P. Morawitz and E. Perez *A Monte Carlo Event Generator for MSSM sparticle production for* e^+e^-, $\mu^+\mu^-$ *and ep colliders* http://lyoinfo.in2p3.fr/susygen/susygen3.html;
E. Perez, Proceedings of the workshop *Monte Carlo Generators for HERA Physics* DESY (1998-1999), 635, A. T. Doyle, G. Grindhammer, G. Ingelmann and H/ Jung (editors).

[26] E. Chabert *et al.*, *QBGFMAR: An Updated Phan package for Cosmic and Halo Muon Topological Rejection in High* P_T *Pysics Analysis*, Technical report, H1, (1998) internal note H1-IN-556

[27] C. Diaconu. *H1EPVEC/2.0* $W^{\pm}$ *and Z production Monte Carlo generator based on EPVEC* (2000)

[28] W. Buchmüller and G. Ingelmann, editors *LPAIR: A Generator for Lepton pair production*, volume 3. DESY, Hamburg (1991) Proceedings of the workshop *Physics at HERA*

[29] T. Sjoestrand *High Energy Event Generation eith PYTHIA 5.7 and JETSET 7.4*, Comp. Phys. Commun. (1994), 82:74-90

[30] H1 Collaboration. *HFS - standard treatment of the hadronic final state*, Part of H1PHAN (PHysical ANalysis) library

[31] H1 Collaboration. *The H1PHAN Manual*, Part of H1PHAN (PHysical ANalysis) library

[32] H1 Collaboration. *QHQTRK - track selection code from the Heavy Flavour PWG* , Part of H1PHAN (PHysical ANalysis) library

[33] H1 Collaboration, Z.Phys. **C67** (1995), 565 and Phys. Lett. **B379** (1996), 319.

[34] G. Martin *Untersuchung von Prozessen des geladenen und neutralen Stroms mit dem H1 Detektor bei HERA* PhD Thesis, University of Hamburg 1997

[35] G. P. Yost *et al.*, Particel Data Group, Phys. Lett. **B204**, 1 (1988)